NASA TECHNICAL MEMORANDUM

NASA TM X-67980

NASA TM X-67980

OXIDATION/VAPORIZATION OF SILICIDE COATED COLUMBIUM BASE ALLOYS

by Fred J. Kohl and Carl A. Stearns
Lewis Research Center
Cleveland, Ohio
December, 1971

This information is being published in preliminary form in order to expedite its early release.

ABSTRACT

Mass spectrometric and target collection experiments have been made at 1600 K to elucidate the mode of oxidative vaporization of two columbium alloys (FS-85 and Cb-752) fused slurry coated with a complex silicide former (Si-20Cr-20Fe). At oxygen pressures up to 5×10^{-4} torr the major vapor component detected by mass spectrometry for oxidized samples was gaseous silicon monoxide. Analysis of condensates collected at oxygen pressures of 0.1, 1.0 and 10 torr revealed that chromium-, silicon-, iron- and tungsten- containing species were the major products of vaporization at these oxygen pressures. Equilibrium thermochemical diagrams were constructed for the metal-oxygen system corresponding to each constituent metal in both the coating and base alloy. The diagrams indicate that the major vaporizing species are expected to be the gaseous oxides of chromium, silicon, iron and tungsten. Plots of vapor phase composition and maximum vaporization rate versus oxygen pressure were calculated for each coating constituent by assuming surface composition, component activities and surface coverage. For a realistic set of these assumptions the major contribution to weight loss by vaporization at oxygen pressures above 1 torr was shown to be chromium-containing species. These results were found to be in general agreement with observed experimental results.

E-6704

OXIDATION/VAPORIZATION OF SILICIDE COATED COLUMBIUM BASE ALLOYS

by Fred J. Kohl and Carl A. Stearns

Lewis Research Center

SUMMARY

Experimental mass spectrometric and target collection measurements were made to elucidate the mode of oxidative vaporization of two oxidation resistant coated columbium alloys. The two alloys studied were FS-85 (Nb-Ta-W-Zr) and Cb-752 (Nb-W-Zr); each alloy was coated by the fused slurry process with a complex silicide former (Si-Cr-Fe).

Under vacuum conditions ($< 10^{-7}$ torr) and at oxygen pressures up to 5×10^{-4} torr, mass spectrometry was used to follow the vaporization at 1570 to 1600 K of both unoxidized and oxidized samples. Unoxidized samples yielded the coating constituents silicon, chromium and iron plus water vapor, carbon monoxide and carbon dioxide. The major vapor component for oxidized samples was silicon monoxide. The only base alloy constituent detected was a very tentative identification of columbium dioxide.

Target collection experiments were performed as a function of oxygen pressure at higher oxygen pressures than were possible in the mass spectrometric studies. Emission spectrographic analysis of the collected condensates revealed that iron-, chromium-, silicon- and tungsten-containing species were the major vapor components.

Using thermodynamic data from the literature, equilibrium thermochemical Kellogg-type diagrams were constructed for assumed simple oxide condensed phase compositions of each constituent in the coating and base alloy. The diagrams indicate that for the assumed equilibrium conditions at 1600 K (2420° F) and oxygen pressures between 10^{-6} and 1 atmosphere, the major vaporizing species are expected to be the gaseous oxides of chromium, silicon, iron and tungsten. The condensed phase oxides of silicon, columbium, iron and tantalum become more stable with respect to vaporization as the oxygen pressure is increased. The vaporization of chromium increases with increasing oxygen pressure while the vaporization of the tungsten and zirconium is oxygen pressure independent. Equations were derived which express the dependence on temperature and oxygen pressure of (1) the vapor pressure of each major vapor phase component, and (2) the condensed state phase boundaries for each system considered.

Plots of vapor phase composition and maximum vaporization rate versus oxygen pressure at 1600 K were made for each coating constituent. These plots were made on the basis of the thermochemical diagrams for assumed surface composition, component activities and surface coverage.

E-6704

At oxygen pressures of interest for practical applications (> 1 torr) and for realistic assumptions of surface coverage and composition, chromium was found to be the major contributor to weight loss and vaporization.

Experimental mass spectrometric and target collection results were found to be in general agreement with vapor composition plots corresponding to a reasonable set of assumptions for surface coverage and component activity. The experimental results are taken as a confirmation of the applicability of the thermodynamic calculations to the actual oxidation/vaporization process. It is felt that the equilibrium vaporization process is a useful approximation to the most severe conditions; these conditions are probably approached at high Mach velocities where the vapor phase will be continuously swept away from the surface.

Cursory consideration from the equilibrium thermodynamic point of view is given to the role of oxygen atoms or water vapor on the oxidative vaporization process. For silicide coatings, water vapor or oxygen atoms should not significantly enhance the loss of material by vaporization.

I. INTRODUCTION

Silicide coated refractory metal alloys are being considered for specific applications involving elevated temperature operation under oxidizing conditions. One such application is the thermal protection system for the reuseable space shuttle. In this application the surface will be subjected to high Mach velocities at temperatures to 1600 K and total pressures in the range from 0.1 to 30 torr. Two of the alloys of particular interest are FS-85 (Nb-27 wt. % Ta-10W-1Zr) and Cb-752 (Nb-10 wt. % W-2.5Zr) coated by a fused slurry process with Si-20 wt. % Cr-20 Fe (ref. 1). The oxidation/vaporization characteristics of the coating under high mass flow conditions may pose a serious problem with respect to high temperature (1600 K (2420° F)) protective and emittance capabilities. Although the oxidation/vaporization behavior of these coated materials has not been well characterized, encouraging results have been obtained from preliminary data from oxidation tests (10 torr static O_2, cyclic self-resistance heating) carried out at the Lewis Research Center (ref. 1). These tests indicate that the Si-Cr-Fe coatings on FS-85 and Cb-752 are stable for more than 100 cycles up to 1683 K. The work reported here was undertaken to help elucidate the oxidative vaporization behavior of these materials by the application of fundamental thermochemical principles and simple experimental methods. The purpose of this report is to present experimentally confirmed calculations of vapor composition developed over Si-20Cr-20Fe coated columbium alloys at 1600 K and reduced pressure. Such data should serve to expose any problems to be anticipated in the high mass flow performance of these coated alloys and will help to establish further definitive experiments for this system.

The past success of oxidation resistant silicide coatings has been attributed to the formation of a passive glassy layer of $SiO_2(c)$ on the external surface which protects the material below from further oxidation. In the last ten years numerous studies have been made of the oxidation/vaporization of simple silicide coated materials, particularly molybdenum and tungsten (ref. 2 and references cited therein). It has been shown that the oxides of molybdenum and tungsten formed by oxidation of the base metal alloy will evaporate more rapidly than the silicon oxide to leave a pure SiO_2 protective glass layer on the surface. Three primary modes of oxidative degradation have been recognized: (1) "silicide pest" which involves oxidation of the intermetallic silicide coating (generally the base metal disilicide) at intermediate temperatures which results in mechanical disintegration of the coating, (2) loss of silicon by vaporization of $SiO(g)$* and $SiO_2(g)$ resulting in coating recession, and (3) interdiffusion and subsequent metal oxide formation causing $SiO_2(c)$ film disruption. In addition to oxidative degradation of the coating, simple vaporization of the coating constituents can occur in vacuum.

For coatings of complex composition (i.e., Sylvania R512E, Si-20 wt. % Cr-20 Fe) the description of the oxidation/vaporization behavior is complicated and not well understood. Formation of the oxides of chromium and iron along with oxides of the substrate elements (Nb, Ta, W, Zr) and mixed oxides such as $(Fe,Cr)NbO_4$ must be considered. The vaporization of chromium as $CrO_3(g)$ is believed to be the major mechanism of weight loss for chromium-containing alloys which form a $Cr_2O_3(c)$ surface layer (refs. 3 and 4 and references cited therein). This may also be a significant factor in the oxidative vaporization of the complex silicide coatings containing chromium. A thermodynamic analysis of the vaporization behavior of the unoxidized and oxidized silicide coated molybdenum base materials has been carried out (refs. 5 to 7); this was possible because thermodynamic data had been obtained previously for the various Mo-Si phases. However, for the complex silicide alloy phases under consideration in the present study, the necessary thermodynamic data for a complete analytical examination have not been experimentally determined.

In order to understand the oxidation/vaporization of the complex silicide coated alloys under various partial pressures of oxygen, it is necessary to know the composition of the vapor phase. The standard types of static furnace tests do not provide the vapor composition data and may give misleading and, at best, not easily interpretable results (refs. 8 to 10). In static or low flow rate furnace tests the vaporization rates are controlled in most cases by diffusion of the vaporizing metal oxides through a vapor phase boundary layer and the diffusion of oxygen to the surface of the sample. Investigations on the vaporization of the chromium oxides illustrate this behavior (refs. 4 and 11). Experimental determinations of

---

*The designation (g) refers to vapor while (c) refers to the condensed phase (solid (s) or liquid (l)).

the vapor composition and vaporization rate at high velocities (up to Mach 12) and low oxygen pressures (0.1 to 100 torr) are difficult and expensive (if not impossible) to carry out. Therefore, experimentally confirmed thermodynamic calculations of vapor composition as presented here should be useful in at least establishing definitive experiments necessary to test satisfactorily and reliably the oxidation/vaporization resistance of the silicide coated columbium alloys under high mass flow conditions.

Parts II and III of this report present experimental results which give a qualitative picture of the oxidative vaporization of the coated alloys under consideration. Mass spectrometric investigations and target collection experiments were carried out to study the composition of the vapor phase.

In part IV of this report we use the thermodynamic data for the elements and oxides of the alloy and coating materials from the literature to calculate equilibrium vapor compositions as a function of temperature and oxygen partial pressure. Insights gained from the experimental study are used with the calculations to arrive finally at a quasi-quantitative description of the vaporization behavior. In part V we consider the effect of oxygen atoms and water vapor on the oxidation/vaporization of the coating and alloy elements.

The results and discussion presented here should also be applicable to other similar coated columbium alloys not specifically investigated (i.e., C129Y). The introduction of additional elements to the coatings or base metal may be handled by the methods described in this report.

II. MASS SPECTROMETRIC STUDIES

A mass spectrometric study of the vaporization of silicide coated Cb-752 and FS-85 was initiated to identify all vaporizing species. A thorough search was made for all possible vaporizing species. Oxidized and unoxidized samples were investigated under both vacuum conditions and at oxygen pressures compatible with the operation of the mass spectrometer.

Experimental Procedure

Samples of each alloy were prepared in the form of strips measuring 0.046x0.25x3.8 cm. The strips were slurry coated with Si-20Cr-20Fe according to the procedure given by Grisaffe and Levine (ref. 12). A photomicrograph of an unoxidized coated FS-85 sample is shown in Fig. 1. The coating, which is approximately 0.008 cm thick, is multi-layered with some cracks extending through to the base alloy. Mass spectrometric results for both alloys were essentially the same as one would expect for samples with identical coatings. Therefore, in discussing the results, no distinction will be made between the two base alloys.

Sample strips were resistively heated by mechanically clamping them between copper electrodes and applying power from a current regulated DC power supply. The surface temperature at the center of the sample was measured with a calibrated Micro Optical brightness pyrometer. Measured temperatures were corrected for the absorption of the viewing window and sample emissivity. Emissivity values of 0.40 and 0.85 were used for the unoxidized and oxidized states, respectively.

The heated sample was contained in a water cooled vacuum chamber which was part of the mass spectrometer inlet system. The modified CEC 21-110 double focusing mass spectrometer has been described in detail previously (refs. 13 and 14). It suffices here to note that electrical detection of ions was used exclusively. Sensitivity was estimated to be between 10^{-10} and 10^{-9} $(gm)(cm^{-2})(sec^{-1})$. Differential pumping made it possible to operate with the maximum pressure in the sample chamber at 2×10^{-4} to 5×10^{-4} torr, a factor of ten higher than that in the ion source chamber. For proper operation of the ion source, maximum pressures in the ion source chamber were limited to 1×10^{-5} to 2×10^{-5} torr; this established the maximum pressure for the sample chamber at about 2×10^{-4} to 5×10^{-4} torr. Although it would be desirable to go to higher pressures for the sample chamber, it was concluded that if additional stages of differential pumping were applied the instrument sensitivity would be decreased significantly by the concomitant increase in the distance from the sample to ion source entrance.

Unoxidized Samples

Initially the vaporization of unoxidized samples was studied under vacuum conditions. Under these conditions the total sample chamber pressure was $< 10^{-7}$ torr as measured with a Bayard-Alpert type ionization gage. The oxygen partial pressure was assumed to be $< 10^{-8}$ torr. When heated to temperatures between 1500 and 1750 K the samples were found to give off CO, H_2O and CO_2. When the temperature was held constant, it was noted that the abundance of these gases decreased with time and eventually they decreased to the normal instrument background level as shown in Fig. 2. Each sample tested showed similar results but the relative abundance of these gases varied from one sample to another. The oxides of carbon are primarily derived from carbon included in the coating during the coating process. Sources are the nitrocelluose lacquer used in slurry application and the 0.1 percent carbon present in the iron powder used. The water vapor is probably adsorbed on the surface.

The gaseous metals Cr, Fe and Si were readily detected during the heating of unoxidized samples. The vaporization rate of these elements varied with time at constant temperature as shown in Fig. 3. Eventually, the abundance of each metal reached a steady value within an order of magnitude of the equilibrium value expected on the basis of the thermodynamic calculations for pure phases. No metals of the base alloy, silicides or oxides were detected during these tests.

In the course of the above experiments it was observed that the appearance of the sample surface changed with time. The surface was monitored with the pyrometer which had a magnification of approximately 3X. Initially the surface appeared uniformly fine grained. As heating progressed the surface appeared to be heterogeneous and took on a mottled structure.

When unoxidized samples were heated for several hours under vacuum and then rapidly exposed and held at an oxygen pressure of 3×10^{-4} torr, the results shown in Figs. 4 and 5 were noted. The CO and CO_2 levels increased but the H_2O level remained constant. The intensity of the CO and CO_2 peaks remained essentially constant while the sample was exposed to the oxygen but when the oxygen was shut off and vacuum conditions were returned, these gases almost instantly decreased to their background levels. These circumstances indicate that the CO and CO_2 were probably formed by a gas-solid reaction.

The levels of Cr, Fe and Si decreased instantaneously when the sample was exposed to oxygen. Cr and Fe were just detectable and Si disappeared completely. At the same time the metals were decreasing, the oxide SiO suddenly appeared and abruptly rose to a level near that predicted by the equilibrium thermodynamic analysis assuming a $SiO_2(s)$ condensed phase on the sample surface. The SiO level for various samples fell within the shaded area shown in Fig. 5.

Equilibrium thermodynamic calculations presented later dictate that if the solid oxide phases are present exclusively the oxide vapors should be detectable and more abundant than the metals. Because Cr and Fe were detected but their oxides were not, one would conclude that these metals were on the surface in an unoxidized state. This condition is unexpected but could be due to insufficient oxygen and/or the preferential reaction of available oxygen at the surface with Si.

During the oxygen exposure a thorough search was made for silicides, Nb, NbO, FeO, CrO_x and SiO_2 but none of these were detected. For one sample a tentative identification of NbO_2 was made.

Following the oxygen exposure the oxygen supply was turned off and the system pressure immediately reduced to $< 10^{-7}$ torr. At this point, the SiO pressure was observed to rise slightly over a period of a few minutes after which the SiO pressure decreased exponentially with time until it was no longer detectable as shown in Fig. 5. As the SiO pressure decreased, the levels of Fe, Cr and Si increased to about those finally attained from samples never exposed to oxygen pressures. All experiments demonstrated that the results of the vacuum - oxygen exposure - vacuum tests could be qualitatively repeated at least for three cycles.

Oxidized Samples

A series of samples were oxidized at high oxygen pressures prior to any testing. Oxidations were completed in situ in the sample vacuum chamber with the mass spectrometer ion source shut off. Oxygen pressures were measured with either a thermistor gage or a dial gage. The system was filled with oxygen to the desired pressure before the sample was heated. Pressure was maintained constant under essentially static conditions during the time of oxidation. Samples were oxidized at 1570 to 1600 K for periods up to 6 hours and at oxygen pressures of 1 and 10 torr. Figure 6 shows a typical cross-section of a sample oxidized at 10 torr. An oxide layer is apparent on the outside surface with some oxide also visible in the cracks in the coating.

Mass spectrometric investigation of oxidized samples under both vacuum conditions and at low oxygen pressures were made with the sample at 1570 to 1600 K. SiO was the major vapor species detected for both conditions. At low oxygen pressures the abundance of SiO(g) remained nearly constant with time. Oxidized samples revealed no trace of any oxides of Cr or Fe but these metals themselves were detected just at the limit of sensitivity of the mass spectrometer. These results suggest that for oxidized samples an extensive SiO_2(c) layer was formed on the surface. This layer was sufficiently extensive to reduce greatly the effective activity of the Cr and Fe present in the coating. Heating of an oxidized sample under vacuum resulted in at least partial depletion of the silicon dioxide layer because the abundance of SiO was noted to decrease with time. After periods of sixteen hours SiO was still detectable and variable with time. As this layer receeded, more surface area containing Cr and Fe became exposed, resulting in increased activity for these metals. On the other hand, when oxidized samples were heated in oxygen atmospheres at pressures down to 3×10^{-4} torr the oxide layer was not depleted. Under both conditions, the loss of base alloy constituents was below the level of detection of the mass spectrometer and as such must be considered as insignificant.

III. TARGET COLLECTION EXPERIMENTS

Target collection experiments were performed to elucidate further the mode of vaporization of silicide coated FS-85. These experiments had the advantage of being performed at much higher pressures of oxygen than was possible in the mass spectrometric studies. While vapor species could not be investigated directly, chemical analysis of the vapor condensate does provide some insights into the vaporization process.

Experimental Procedure

These experiments were carried out in the mass spectrometer sample chamber with samples similar to those used in the mass spectrometer

studies. A platinum collector attached to a water cooled plate was placed in front of the sample and about 1.3 cm away. After the chamber was thoroughly evacuated ($\leq 10^{-7}$ torr) the pump was valved off and oxygen was admitted to the chamber. Pressure in the chamber was maintained by regulating the leak rate of oxygen into the chamber. For all practical purposes this was a static condition. Once the oxygen was stabilized, heating of the sample was begun. At the completion of each experiment the sample was cooled prior to removal of the platinum collector from the system.

Target collections were made by heating coated alloy samples for 6 hours at 1570 to 1600 K at oxygen pressures of 0.1, 1.0 and 10.0 torr. The collected condensate ranged in weight from 0.3 to 2.0 milligram. The condensate collected on the platinum was analyzed by a technique using sodium tetraborate-sodium nitrate fusion. The condensate film was dissolved by fusion with an evaporated tetraborate-nitrate solution and washed off the platinum collector. Analysis was performed by an emission spectroscopic technique (ref. 15). The results tabulated in table I were obtained after the first collection on a new sample for each experiment. The accuracy of the chemical analysis is expected to be approximately ±10 percent of the value reported. These results are plotted versus oxygen pressure in Fig. 7 along with the observed Si-Cr-Fe ratio from the mass spectrometric experiments. The high silicon and low iron concentrations at the lower pressure indicate that the main fraction of the surface is covered by silicon oxide. The fact that some of the base alloy metal constituents were detected in the collected condensate indicates that these materials are present on the surface of oxidized samples.

IV. CALCULATION OF VAPOR COMPOSITION

Thermochemical Diagrams

To describe quantitatively the equilibrium mode of vaporization of each metal and its oxides in various oxidizing atmospheres, one must know the partial pressures of all vapor species involved as a function of condensed phase composition, temperature and oxygen pressure. The thermochemical diagrams first described by Kellogg (ref. 16) and later extended by Gulbransen and Jansson (refs. 17 to 19) provide a convenient method for presentation of such information.

For the metals being considered here their condensed state oxides and vapor species are listed in table II. Chemical reactions describing the various condensed state-vapor equilibria are presented in table III. The phase boundaries listed in table IV and vapor pressures listed in table V for each species were calculated by use of the chemical reactions and pertinent thermochemical relations. The procedure followed is given in appendix A where the calculation of the partial pressures of SiO(g) is used as an example.

Figures 8 to 14 present the thermochemical diagrams constructed by the method outlined. The diagrams show the logarithm of the pressure of the various metal-oxygen species plotted versus the logarithm of the oxygen pressure. The vertical line in each diagram designates the boundary between the respective condensed phases. All the diagrams shown are for a temperature of 1600 K. These diagrams are discussed in detail in appendix B.

Vaporization Rate

The vapor pressures (P_i) given in the thermochemical diagrams may be used to calculate the equilibrium or maximum possible rate of vaporization of any species, i. The Hertz-Langmuir equation is used to calculate the rate of weight loss per unit area G_i:

$$G_i(\mathrm{gm/cm^2/sec}) = \frac{P_i(\mathrm{atm})}{2.255\times10^{-2}} \left(\frac{M_i(\mathrm{gm/mole})}{T(\mathrm{K})}\right)^{1/2} \tag{1}$$

The rate of evaporation of a metal due to vaporization of an oxide species can be obtained from equation (1) by multiplying by the molecular weight ratio $(M_{metal}/M_i)^{1/2}$:

$$G_{metal}(\mathrm{gm/cm^2/sec}) = \frac{P_i(\mathrm{atm})}{2.255\times10^{-2}} \left(\frac{M_{metal}(\mathrm{gm/mole})}{T(\mathrm{K})}\right)^{1/2} \tag{2}$$

The actual weight loss of metal depends not only on the vapor pressures of the major molecular species but also on the percentage of surface area of the particular metal or oxide exposed and its activity.

Application to Silicide Coatings

The real behavior of silicide coated columbium alloys under high temperature oxidizing conditions is much more complex than the idealized scheme given above and discussed in appendix B for simple oxides. It must be emphasized that equilibrium vaporization rates are intended to serve only as first estimates of vaporization behavior. While such first estimates are essential to an understanding of the process, one must remember that kinetic effects, diffusion, modifications of and anomalies in the surface composition may profoundly influence the actual vaporization behavior. Nevertheless, it is felt that the equilibrium vaporization process may be a reasonable approximation to the worst possible behavior; this behavior will be approached at high Mach velocities when the vapor phase will be continuously swept away from the surface of the oxidized coating.

For the coatings and base alloys being considered here, further complications arise due to the formation of complex metal silicides of the type MSi_2 and M_5Si_3 (ref. 2). The oxidation of the coating to give an SiO_2 protective layer may still predominate but consideration must be given to complex oxides or spinels. The formation of oxides such as $NbCrO_4$, $FeCr_2O_4$, Cr_2SiO_4, $(Fe,Cr)NbO_4$ and others should, however, be beneficial. The supposedly negative free energies of formation of these compounds from the simple oxides would tend to stabilize the condensed phases of the more volatile metals with respect to vaporization. Also, the lowering of the activities of the metals or oxides by the formation of alloys and/or complex phases, should result in proportional reductions in the vaporization rate. The effective vaporization rate of any element would be determined by both the activity of the metal or metal oxide and its ability to diffuse to the external surface of the coating.

The thermochemical diagrams can be used along with estimates of the composition of the surface and component activities to calculate the composition of the vapor phase and rate of weight loss as a function of temperature and oxygen pressure. The results of several calculations of this type for the systems being considered here are given in Figs. 15 to 19. For the calculations we assumed that the elements Si, Cr and Fe exist as the equilibrium determined oxides on the surface of the coated alloy; all remaining elements were ignored. The calculations were made for various combinations of surface coverage and component activities to show the changes produced by these parameters.

Initially, we assumed fractional surface area coverages corresponding to the proportions of the elements in the slurry used to produce the coating. The fractions for the oxides of Si, Cr and Fe used were 0.6, 0.2 and 0.2, respectively. Unit activity was assumed for $SiO_2(c)$, $Cr_2O_3(c)$, $Fe_2O_3(c)$, $Fe_3O_4(c)$ and $FeO(c)$. The vapor composition plots for these conditions are given in Fig. 15. At high oxygen pressures Cr is seen to be the only significant metal component in the vapor phase. At intermediate low oxygen pressures both Cr and Fe make up the bulk of the metal components in the vapor. For the lowest oxygen pressures Fe predominates with only approximately a 10 percent contribution from the Si-containing species. A comparison of Fig. 15 with the experimental data given in Fig. 7 shows that the assumed conditions do not apply. This is not unexpected because the mass spectrometry results indicate that the surface is mostly $SiO_2(c)$ with very little Fe- and Cr-oxides and thus the assumed fractional surface coverages are recognized as unrealistic.

The plots shown in Figs. 16 and 17 assumed $SiO_2(c)$ surface coverage fractions of 0.99 and 0.999, respectively, with the Fe-and Cr-oxide fractions being equal and making up the remainder of the surface. Again, unit activity was assumed for each component. These conditions are expected to more closely approach actual conditions and indeed these figures are in better agreement with Fig. 7 which shows the experimentally

obtained results. For Figs. 16 and 17, Cr-containing species are seen to still predominate at the highest oxygen pressures. However, at the lowest oxygen pressures Si-containing species are most abundant as contrasted to Fig. 15 where the Fe dominated at the low oxygen pressures. In the range of surface coverage fractions used for Figs. 16 and 17 the abundance of Fe-containing species is quite critically dependent on the specific fractions assumed. At the present time it is not possible a priori to make a judicious choice of surface coverage fractions. Furthermore, in the real situation surface coverage may not be constant.

The effect of varying component activities is shown in Figs. 18 and 19. Reducing the activity of each oxide phase from unity to 0.1 results in marked changes in the vapor composition. The Si abundance is reduced by a factor of 0.1 whereas the Cr species are reduced by $(0.1)^{1/2}$ and the Fe species are reduced by $(0.1)^{1/2}$, $(0.1)^{1/3}$ and 0.1, respectively, for the three compositions Fe_2O_3, Fe_3O_4 and FeO.

The estimated rate of total metal weight loss from the coating for each condition corresponding to Figs. 15 to 19 is presented in Fig. 20. Maximum weight loss occurs at the highest oxygen pressures and the minimum weight loss occurs at oxygen pressures in the range of about 10^{-4} to 10^{-6} atm. These figures show that the total weight loss is a complicated function of the surface coverage and component activity. The real weight loss expected for the coated alloys in the actual pressure environment is estimated to be within an order of magnitude of the region between curves c to e in Fig. 20. This expectation is based on the agreement between the experimental results of Fig. 7 and the calculated curves in Figs. 17 to 19. Assuming that Fig. 19 represents the actual surface condition, the weight loss per unit area for a shuttle surface exposed to 100 cycles of 0.5 hour duration at 5 torr oxygen partial pressure at 1600 K, would be 1.4×10^{-4} gm/cm^2. Approximately 90 percent of this weight loss would be chromium with the remainder due to silicon.

V. EFFECT OF OXYGEN ATOMS AND WATER VAPOR

Oxidation in the Presence of Atomic Oxygen

Some metals exhibit greatly increased rates of oxidation upon reaction with dissociated or atomic oxygen (O·) as compared with their reactions with molecular O_2 (refs. 28 and 29). Because relatively high concentrations of atomic oxygen are formed under the conditions of atmospheric reentry of a body such as the proposed space shuttle vehicle, the oxidation by atomic oxygen of the coatings and alloys proposed for use in the thermal protection system of such a vehicle is of interest. Rosner and Allendorf (ref. 28) have recently reviewed the literature concerning the kinetics of the attack of refractory materials by dissociated gases. For metals such as molybdenum and tungsten which do not form protective oxide layers, reactant gas dissociation leads to order-of-magnitude

enhancements in reaction rates. For elements such as silicon which form semi-protective surface films of stable oxide, only minor changes in reaction rate are observed. Surprisingly, atomic oxygen leads to a suppression of the rate of oxidation of silicon carbide and favorably effects the conditions necessary to maintain a passive $SiO_2(c)$ film on the surface (refs. 28 and 30). A $SiO_2(c)$ surface layer on the coated columbium alloys is expected to exhibit similar behavior.

Recent experimental studies of the oxidation of chromium-containing alloys by atomic oxygen carried out by Gilbreath (ref. 31) have shown that the oxidative vaporization of $Cr_2O_3(c)$ to $CrO_3(g)$ is enhanced by comparison to rates of oxidation measured with molecular O_2. No experimental data exist for the action of atomic oxygen on the other coating or alloy constituents, Fe, Nb, Ta and Zr. It appeared to be of interest at this point to construct the equilibrium thermochemical diagrams for reactions involving oxygen atoms. Using the methods outlined in the appendix, diagrams were constructed for the silicon, chromium and iron oxide systems (Figs. 21 to 23). Comparison of the oxygen atom equilibrium diagrams to those for molecular oxygen for the silicon and chromium oxide systems can lead to a simple rationalization of the experimental results. The general features of the oxygen atom diagrams are essentially the same as those for the molecular oxygen. For the atomic oxygen cases the phase boundaries are shifted. The real significant differences are the behavior of the pressure dependent molecular species at high oxygen pressures. For the silicon-oxygen system the rate of change of the SiO(g) pressure as a function of oxygen pressure is more negative for the atomic oxygen than molecular oxygen. Since the $SiO_2(g)$ is still pressure independent, the net result of going from molecular to atomic oxygen is a slight decrease in total pressure of silicon-containing species. The experimental results of Rosner and Allendorf (ref. 30) are in qualitative agreement with this behavior. For the chromium-oxygen system it is obvious that oxygen atoms greatly enhance the volatility of the major chromium-containing species above 10^{-9} atm. The experimental results of Gilbreath (ref. 31) appear to be in qualitative agreement with what one would predict on the basis of thermochemical claculations.

For the iron-oxygen system the effect of oxygen atoms is to decrease the partial pressure of Fe(g) and FeO(g). The stability of the columbium, tantalum and zirconium condensed state oxides, similar to those of silicon and iron, may prevent the enhancement of oxidation by atomic oxygen.

It must be emphasized here that the thermochemical diagrams for oxygen atoms describe the equilibrium reaction between the respective condensed phases and oxygen atoms. However, the recombination of atoms on the surface to form oxygen molecules may be the predominant reaction in some systems and this will be an important consideration. Such a reaction would produce significantly less enhancement of vaporization due to oxygen atoms than that predicted by the thermochemical diagrams. Definitive descriptions of the role of oxygen atoms in the oxidative vaporization of complex silicide coatings will require further experimental results.

Equilibrium Vaporization in the Presence of Water Vapor

For certain applications the role of water vapor on the oxidative vaporization of silicide coated alloys is of interest. Belton and associates (refs. 23 and 32 to 34) have examined the enhanced volatility of several metal oxides in the presence of $H_2O(g)$. They have attributed the increase in vaporization weight loss of metal to the formation and subsequent vaporization of such gaseous hydroxides as $CrO_2(OH)$, $Fe(OH)_2$, $WO_2(OH)_2$ and $MoO_2(OH)_2$ by the reactions:

$$Cr_2O_3(c) + O_2(g) + H_2O(g) = 2CrO_2(OH)(g)$$

$$Fe_2O_3(c) + 2H_2O(g) = 2Fe(OH)_2(g) + \frac{1}{2} O_2(g)$$

$$WO_3(c) + H_2O(g) = WO_2(OH)_2(g)$$

$$MoO_3(c) + H_2O(g) = MoO_2(OH)_2(g)$$

Calculations of the type shown above could also be made for hydroxide species, giving their concentrations as a function of oxygen and water vapor gas pressure. For example, calculations of the pressures of $CrO_2(OH)(g)$ demonstrate that this species will be important in the vaporization of $Cr_2O_3(c)$ in atmospheres containing both $O_2(g)$ and $H_2O(g)$ (ref. 3). At 1273 K with the pressures of $O_2(g)$ and $H_2O(g)$ both equal to 10^{-2} atm, the equilibrium pressure of $CrO_2(OH)(g)$ is 2.2 times greater than that of $CrO_3(g)$.

No gaseous hydroxides have been reported for Si, Nb, Ta or Zr up to the present time. Therefore, it is presumed that the action of water vapor will be relatively unimportant if the external oxidized surface coating is mainly $SiO_2(c)$. Conversely, coating or alloy recession would be enhanced if chromium, iron or tungsten oxides were exposed to oxygen-water vapor gas mixtures at elevated temperatures.

VI. SUMMARY AND CONCLUDING REMARKS

Experimental mass spectrometric and target collection measurements were made to elucidate the mode of oxidative vaporization of two oxidation resistant coated columbium alloys. The two alloys studied were FS-85 (Nb-Ta-W-Zr) and Cb-752 (Nb-W-Zr); each alloy was coated by the fused slurry process with a complex silicide former (Si-Cr-Fe).

Under vacuum conditions ($< 10^{-7}$ torr) and at oxygen pressure up to 5×10^{-4} torr, mass spectrometry was used to follow the vaporization at

1570 to 1600 K of both unoxidized and oxidized samples. Unoxidized samples yielded the coating constituents silicon, chromium and iron plus water vapor, carbon monoxide and carbon dioxide. The major vapor component for oxidized samples was silicon monoxide. The only base alloy constituent detected was a very tentative identification of columbium dioxide.

The mass spectrometric results at 1600 K lead to the following conclusions: (1) exposure of the heated sample to oxygen pressures as low as 3×10^{-4} torr results in a surface coverage which is predominantly $SiO_2(c)$; (2) the $SiO_2(c)$ surface coverage is maintained at low oxygen pressures and only lost in vacuum after considerable time; (3) samples oxidized at high oxygen pressures have a more complete surface coverage of $SiO_2(c)$; and (4) base alloy or other coating constituents besides Si are not present at the surface in significant abundance either as the metal or simple oxide.

Target collection experiments were performed as a function of oxygen pressure at higher oxygen pressures than were possible in the mass spectrometric studies. Emission spectrographic analysis of the collected condensates revealed that iron, chromium, silicon and tungsten were the major vapor components.

The suggested picture of a protective surface layer of $SiO_2(c)$ is not unequivocally verified by the experimental results. The target collection results indicate that all constituent elements of both the coating and base alloy are able to vaporize from the sample. This leads one to postulate that while the oxidized surface is mainly $SiO_2(c)$, the protective layer is not complete and/or impervious. The loss of base alloy constituents does not appear to be a serious problem except possibly in the case of tungsten. The results given here indicate that in shuttle applications the principal components lost will be chromium and lesser amounts of tungsten under high mass flow external pressure conditions. For expected internal pressure conditions silicon, chromium, iron and tungsten will be lost, but not at rates approaching that determined by equilibrium vapor pressures because the internal environment is relatively static.

Using thermodynamic data from the literature, equilibrium thermochemical Kellogg-type diagrams were constructed for assumed simple oxide condensed phase compositions of each constituent in the coating and base alloy. The diagrams indicate that for the assumed equilibrium conditions at 1600 K (2420° F) and oxygen pressures between 10^{-6} and 1 atmosphere, the major vaporizing species are expected to be the gaseous oxides of chromium, silicon, iron and tungsten. The condensed phase oxides of silicon, columbium, iron and tantalum become more stable with respect to vaporization as the oxygen pressure is increased. The vaporization of chromium increases with increasing oxygen pressure while the vaporization of tungsten and zirconium is oxygen pressure independent. Equations

were derived which express the dependence on temperature and oxygen pressure of (1) the vapor pressure of each major vapor phase component, and (2) the condensed state phase boundaries for each system considered.

Plots of vapor phase composition and maximum vaporization rate versus oxygen pressure at 1600 K were made for each coating constituent. These plots were made on the basis of the thermochemical diagrams for assumed surface composition, component activities and surface coverage. At oxygen pressures of interest for practical applications (> 1 torr) and for realistic assumptions of surface coverage etc., chromium was found to be the major contributor to weight loss and vaporization.

The conclusions arrived at as a result of the mass spectrometric experiments lend credence to several of the assumptions used in calculating the vapor composition plots presented. Simple oxide condensed phase compositions were used in constructing the thermochemical diagrams and this is apparently correct at least for the constituent element silicon. Surface coverage was assumed to be mainly $SiO_2(c)$ and its activity was considered to be near unity for the vapor composition plot shown in Fig. 19. This figure is seen to be in general agreement with Fig. 7 where both the experimental target collection and mass spectrometric results are plotted. The degree of agreement between these figures is considered to be good. Perfect agreement might possibly be achieved by suitably adjusting the surface coverage and activity parameters but there is no a priori reason for making such adjustments.

Cursory considerations from the equilibrium thermodynamic point of view were given to the role of oxygen atoms or water vapor on the oxidative vaporization of silicide coating constituents. These considerations indicate that oxygen atoms should not significantly enhance the loss of material by oxidative vaporization.

The idealized equilibrium thermochemical calculations presented here have been shown to be in general agreement with actual behavior observed experimentally. It should be obvious that a need exists for the identification of the surface oxide phases formed under various conditions for the complex silicide coated alloys. With this information a much more certain description of the oxidative vaporization process would be possible. Nevertheless, it is apparent from this study that analytical thermochemical considerations establish general patterns of behavior and point out any exceptional behavior. The results presented here are considered to be sufficiently conclusive to emphasize that equilibrium thermodynamics is an appropriate starting point when considering the oxidative vaporization of any system regardless of its complexity.

APPENDIX A

The procedure followed to construct the thermochemical diagrams is outlined here using the SiO(g) species as an example.

Three chemical reactions are considered:

$$(1) \quad Si(c) + O_2(g) = SiO_2(c)$$

$$(2) \quad Si(c) + \tfrac{1}{2} O_2(g) = SiO(g)$$

$$(3) \quad SiO_2(c) = SiO(g) + \tfrac{1}{2} O_2(g)$$

Reaction (1) is used to describe the phase boundary between Si(c) and SiO_2(c) while reactions (2) and (3) are needed to determine the vapor pressures of SiO(g). The equilibrium constant K for each reaction is defined as the ratio of the product of the activities of the reaction products to the product of the activities of the reactants. Because the activity of a gas component can be approximated by its partial pressure, the equilibrium constants for reactions (1), (2) and (3) may be written, respectively, as:

$$K_{(1)} = \frac{a_{SiO_2(c)}}{a_{Si(c)} P_{O_2(g)}} \tag{A1a}$$

$$K_{(2)} = \frac{P_{SiO(g)}}{a_{Si(c)} P_{O_2(g)}^{1/2}} \tag{A2a}$$

$$K_{(3)} = \frac{P_{SiO(g)} P_{O_2(g)}^{1/2}}{a_{SiO_2(c)}} \tag{A3a}$$

where a_i represents the activity and P_i the partial pressure of component i. By taking logarithms, (A1a), (A2a) and (A3a) may be written in the alternate form:

$$\log K_{(1)} = \log a_{SiO_2(c)} - \log a_{Si(c)} - \log P_{O_2(g)} \tag{A1b}$$

$$\log K_{(2)} = \log P_{SiO(g)} - \log a_{Si(c)} - \tfrac{1}{2} \log P_{O_2(g)} \tag{A2b}$$

$$\log K_{(3)} = \log P_{SiO(g)} + \frac{1}{2} \log P_{O_2(g)} - \log a_{SiO_2(c)} \qquad \text{(A3b)}$$

For any chemical reaction, r, $\log K_r = \Sigma \log K_p$ (products) - $\Sigma \log K_p$ (reactants), where K_p is the equilibrium constant for the formation reaction of the various constituents from pure elements in their standard states. Therefore, $\log K_r$ for reactions (1), (2) and (3) can be expressed in terms of the $\log K_p$ for the components:

$$\log K_{(1)} = \log K_{p,SiO_2(c)} - \log K_{p,Si(c)} - \log K_{p,O_2(g)} \qquad \text{(A1c)}$$

$$\log K_{(2)} = \log K_{p,SiO(g)} - \log K_{p,Si(c)} - \frac{1}{2} \log K_{p,O_2(g)} \qquad \text{(A2c)}$$

$$\log K_{(3)} = \log K_{p,SiO(g)} + \frac{1}{2} \log K_{p,O_2(g)} - \log K_{p,SiO_2(c)} \qquad \text{(A3c)}$$

By combining Eqs. (A1b), (A2b) and (A3b) with (A1c), (A2c) and (A3c), respectively, the pressures of the various gaseous species are obtained in terms of the $\log K_p$'s, activities of the condensed phase components, and pressures of oxygen gas:

at the Si(c)-SiO_2(c) phase boundary,

$$\log P_{O_2(g)} = \log K_{p,Si(c)} + \log K_{p,O_2(g)} - \log K_{p,SiO_2(c)} + \log a_{SiO_2(c)} - \log a_{Si(c)} \qquad \text{(A1d)}$$

in the Si(c) phase,

$$\log P_{SiO(g)} = \log K_{p,SiO(g)} - \log K_{p,Si(c)} - \frac{1}{2} \log K_{p,O_2(g)} + \log a_{Si(c)} + \frac{1}{2} \log P_{O_2(g)} \qquad \text{(A2d)}$$

and in the SiO_2(c) phase,

$$\log P_{SiO(g)} = \log K_{p,SiO(g)} + \frac{1}{2} \log K_{p,O_2(g)} - \log K_{p,SiO_2(c)} - \frac{1}{2} \log P_{O_2(g)} + \log a_{SiO_2(c)} \qquad \text{(A3d)}$$

Because Si(c) and O_2(g) are the standard states for silicon and oxygen in the temperature range being considered, log K_p for these species is zero by definition. For unit activity of the condensed phases, log a terms are also zero. Therefore, Eqs. (A1d), (A2d) and (A3d) in the respective phases reduce to:

$$\log P_{O_2(g)} = - \log K_{p,SiO_2(c)} \qquad \text{(A1e)}$$

$$\log P_{SiO(g)} = \log K_{p,SiO(g)} + \frac{1}{2} \log P_{O_2(g)} \qquad \text{(A2e)}$$

$$\log P_{SiO(g)} = \log K_{p,SiO(g)} - \log K_{p,SiO_2(c)} - \frac{1}{2} \log P_{O_2(g)} \qquad \text{(A3e)}$$

Numerical values of log K_p for most of the species listed in table I are tabulated as a function of temperature in the literature sources listed.

APPENDIX B

Each of the thermochemical diagrams for the single metal-oxygen systems is discussed here in relation to surface oxidation/vaporization.

The most striking feature evident in the diagram for the silicon-oxygen system (Fig. 8) is the high vapor pressure of SiO(g) at the Si(c)-SiO_2(c) phase boundary where the equilibrium oxygen pressure is quite low. This circumstance strongly influences the kinetics and mechanism of oxidation for elemental silicon or metal silicides. Under equilibrium conditions at high oxygen pressures (10^{-6} to 1 atm) both SiO(g) and SiO_2(g) are vaporization products but their equilibrium partial pressures are sufficiently low (< 10^{-10} atm) so as to make silicon losses insignificant as far as practical applications are concerned. Therefore, a complete surface coating of SiO_2(c) should be acceptable from the standpoint of simple vaporization. However, the high SiO(g) pressure at the metal-oxide interface could be the cause of problems. For example, if the surface oxide coating is porous, SiO(g) can rapidly diffuse to the surface where it can either vaporize or form SiO_2(c) smoke by reaction with oxygen. Alternately, the high SiO(g) pressure at the interface may lead to cracking and rupture of the surface coating if the external pressure is lower than that of the SiO(g). The pressures (and diffusion coefficients) of SiO(g) and oxygen also determine the transition between so called active (rapid) and passive (slow) oxidation. In general, a passive SiO_2(c) layer is formed if the oxygen pressure is greater than the SiO(g) pressure (ref. 17 and references cited therein).

From the diagram for the chromium-oxygen system (Fig. 9) it is apparent that the situation is somewhat different from that for the silicon-oxygen system. Here, the pressures of the gaseous species CrO_3(g) and CrO_2(g) increase as the oxygen pressure increases over the condensed phase Cr_2O_3(c). This characteristic could be especially detrimental for some practical applications and could lead to very significant weight losses. Coupled to this is another feature shown in Fig. 9. The high value of the Cr(g) pressure over Cr(c) may lead to increased transport of chromium to the surface where it can oxidize and further contribute to loss of chromium. The consequences of the high CrO_3(g) pressure with respect to vaporization losses has been previously discussed (refs. 3, 4 and references cited therein) for chromium-containing alloys.

From Fig. 10 it is to be noted that although the volatility of Fe(g) is relatively high over the Fe(c) phase the trend with respect to increasing oxygen pressure over the oxide phases is to stabilize the condensed phases. At oxygen pressures in the range from 10^{-6} to 1 atmosphere, losses of iron are not expected to be severe due to the low pressures of the vaporizing components Fe(g) and FeO(g).

The diagrams for the oxygen systems of Nb, Ta and Zr are all similar and show that the dioxide species are the predominant vapor phase component at high oxygen pressures. The Nb and Ta solid oxides are both stabilized by increasing oxygen pressure while the vaporization of $ZrO_2(g)$ is independent of oxygen pressure over the $ZrO_2(c)$ phase. At 1600 K the loss of any of these refractory metals by evaporation will be almost insignificant at the oxygen pressures being considered here because the vapor pressures of the respective metal oxides are exceedingly low.

The diagram for the tungsten-oxygen system is considerably different from those considered above. Over the tungsten oxide condensed phases the vapor components include several polymers of the form $(WO_3)_x$. These species have relatively high vapor pressures which are independent of oxygen pressure in the range of practical consideration. For this system loss of tungsten by evaporation will be pronounced because of the many polymers and their high vapor pressures. Losses due to the dioxide gas will, however, be insignificant. This behavior is analogous to that observed in the Mo-O system (refs. 2 and 5).

REFERENCES

1. Grisaffe, S. J.; Merutka, J. P.; and Levine, S. R.: A Status Review of Lewis Research Center Supported Protection System Development. NASA TM X-52977, 1971.

2. Pound, G. M.; Jaffee, R. I.; and Perkins, R. A., eds.: High Temperature Oxidation-Resistant Coatings. Rep. NMAB-263, National Materials Advisory Board (NASA CR-110452), May 1970, pp. 22-57, 141-148.

3. Kohl, Fred J.; and Stearns, Carl A.: Vaporization of Chromium Oxides from the Surface of TD NiCr under Oxidizing Conditions. NASA TM X-52879, 1970.

4. Graham, H. C.; and Davis, H. H.: Oxidation/Vaporization Kinetics of Cr_2O_3. J. Am. Ceram. Soc., vol. 54, no. 2, Feb. 1971, pp. 89-93.

5. Bartlett, R. W.: Investigation of Mechanisms for Oxidation Protection and Failure of Intermetallic Coatings for Refractory Metals. Rep. U-3267, Aeronutronic (ASD-TDR-63-753, Pt. III, AD-472919), Oct. 14, 1965.

6. Bartlett, R. W.; and Gage, P. R.: Investigation of Mechanisms for Oxidation Protection and Failure of Intermetallic Coatings for Refractory Metals. Rep. U-2660, Aeronutronic (ASD-TDR-63-753, Pt. II, AD-609167), July 1964.

7. Berkowitz-Mattuck, Joan B.; and Dils, R. R.: High-Temperature Oxidation. II. Molybdenum Silicides. J. Electrochem. Soc., vol. 112, no. 6, June 1965, pp. 583-589.

8. Fryburg, George C.; and Murphy, Helen M.: On the Use of Furnaces in the Measurement of the Rate of Oxidation of Platinum and Other Metals Forming Volatile Oxide. Trans. AIME, vol. 212, no. 5, Oct. 1958, pp. 660-661.

9. Fryburg, George C.; and Petrus, Helen M.: Kinetics of the Oxidation of Platinum. J. Electrochem. Soc., vol. 108, no. 6, June 1961, pp. 496-503.

10. Turkdogan, E. T.; Grieveson, P.; and Darken, L. S.: Enhancement of Diffusion-Limited Rates of Vaporization of Metals. J. Phys. Chem., vol. 67, no. 8, Aug. 1963, pp. 1647-1654.

11. Lowell, Carl E.: A Scanning Electron Microscope Study of the Surface Morphology of TD-NiCr Oxidized at 800° to 1200° C. NASA TM X-67867, 1971.

12. Grisaffe, S. J.; and Levine, S. R.: Private Communication.

13. Stearns, Carl A.; and Kohl, Fred J.: The Dissociation Energy of Gaseous Titanium Mononitride. NASA TN D-5027, 1969.

14. Kohl, Fred J.; and Stearns, Carl A.: Mass Spectrometric Investigation of Vaporization Thermodynamics of Yttrium Dicarbide-Carbon System and Dissociation Energy of Yttrium Dicarbide and Tetracarbide. NASA TN D-5646, 1970.

15. Gordon, W. A.; and Chapman, G. B.: Quantitative Direct-Current Arc Analysis of Random Compositions of Microgram Residues in Silver Chloride Common Matrix. Spectrochim. Acta, Pt. B: Atomic Spectroscopy, vol. 25, no. 3, Mar. 1970, pp. 123-138.

16. Kellogg, H. H.: Vaporization Chemistry in Extractive Metallurgy. Trans. AIME, vol. 236, no. 5, May 1966, pp. 602-615.

17. Gulbransen, Earl A.; and Jansson, Sven A.: Vaporization Chemistry in the Oxidation of Carbon, Silicon, Chromium, Molybdenum and Niobium. Heterogeneous Kinetics at Elevated Temperatures. G. R. Belton and W. L. Worrell, eds., Plenum Press, 1970, pp. 181-208.

18. Jansson, S. A.; and Gulbransen, E. A.: Evaluation of Gas-Metal Reactions by Means of Thermochemical Diagrams. Extended Abstracts of the 4th International Congress on Metallic Corrosion, Amsterdam, Netherlands, Sept. 7-14, 1969, p. 77.

19. Gulbransen, Earl A.: Thermochemistry and the Oxidation of Refractory Metals at High Temperature. Corrosion, vol. 26, no. 1, Jan. 1970, pp. 19-28.

20. Stull, D. R., ed.: JANAF Thermochemical Data. Dow Chemical Co., Midland, Mich., All Supplements Issued to Date.

21. Wicks, C. E.; and Block, F. E.: Thermodynamic Properties of 65 Elements-Their Oxides, Halides, Carbides and Nitrides. Bull. 605, U.S. Bureau of Mines, 1963.

22. Schick, H. L., ed.: Thermodynamics of Certain Refractory Compounds. Academic Press, 1966.

23. Kim, Y.: Volatilization of Chromic Oxide in Oxygen and Water Vapor. Ph. D. Thesis, Univ. Pennsylvania, 1969. G. B. Belton, advisor.

24. Porter, Richard F.; Chupka, William A.; and Inghram, Mark G.: Mass Spectrometric Study of Gaseous Species in the Si-SiO_2 System. J. Chem. Phys., vol. 23, no. 1, Jan. 1955, pp. 216-217.

25. McDonald, J. D.; and Margrave, J. L.: Mass Spectrometric Studies at High Temperatures XVI. Sublimation and Vaporization of Chromium Trioxide. J. Inorg. Nucl. Chem., vol. 30, no. 2, Feb. 1968, pp. 665-667.

26. Kant, Arthur; and Strauss, Bernard: Dissociation Energy of Cr_2. J. Chem. Phys., vol. 45, no. 8, Oct. 15, 1966, pp. 3161-3162.

27. Lin, Sin-Shong; and Kant, Arthur: Dissociation Energy of Fe_2. J. Phys. Chem., vol. 73, no. 7, July 1969, pp. 2450-2451.

28. Rosner, Daniel E.; and Allendorf, H. D.: Kinetics of the Attack of Refractory Materials by Dissociated Gases. Heterogeneous Kinetics at Elevated Temperatures. G. R. Belton and W. L. Worrell, eds., Plenum Press, 1970, pp. 231-251.

29. Fryburg, George C.: Enhanced Oxidation of Platinum in Activated Oxygen. J. Chem. Phys., vol. 24, no. 2, Feb. 1956, pp. 175-180. Fryburg, George C.: Enhanced Oxidation of Platinum in Activated Oxygen. II. Identity of Active Species and Oxide Formed. J. Chem. Phys., vol. 42, no. 11, June 1, 1965, pp. 4051-4052. Fryburg, George C.: Enhanced Oxidation of Platinum in Activated Oxygen. III. Kinetics and Mechanism. J. Phys. Chem., vol. 69, no. 10, Oct. 1965, pp. 3660-3662.

30. Rosner, Daniel E.; and Allendorf, H. Donald: High Temperature Kinetics of the Oxidation and Nitridation of Pyrolytic Silicon Carbide in Dissociated Gases. J. Phys. Chem., vol. 74, no. 9, Apr. 30, 1970, pp. 1829-1839.

31. Gilbreath, William P.: Preliminary Studies of the Oxidation of TD Ni-20Cr in Static, Flowing, and Dissociated Oxygen at 1100° C and 130 Nm^{-2}. NASA TM X-62064, 1971.

32. Belton, G. R.; and Richardson, F. D.: A Volatile Iron Hydroxide. Trans. Faraday Soc., vol. 58, 1962, pp. 1562-1572.

33. Belton, G. R.; and McCarron, R. L.: The Volatilization of Tungsten in the Presence of Water Vapor. J. Phys. Chem., vol. 68, no. 7, July 1964, pp. 1852-1856.

34. Belton, G. R.; and Jordan, A. S.: The Volitilization of Molybdenum in the Presence of Water Vapor. J. Phys. Chem., vol. 69, no. 6, June 1965, pp. 2065-2071.

TABLE I. - WEIGHT PERCENT OF METALS FROM TARGET COLLECTION EXPERIMENTS

[FS-85 coated with Si-20 wt. % Cr-20 Fe. Heated for 6 hours at 1570-1600 K.]

Metal	Oxygen pressure, torr		
	10.0	1.0	0.1
Fe	2.6	31.0	29.3
Cr	91.1	54.1	13.7
Si	2.6	3.2	36.4
W	3.3	11.4	19.7
Nb	<.09	.21	.81
Ta	~.3	<.03	<.03
Zr	<.09	<.02	<.02

TABLE II. - ELEMENTS AND OXIDES CONSIDERED IN THE CALCULATIONS AND SOURCES OF THERMODYNAMIC DATA

Element	Condensed phase oxide	Possible high temperature vapor species
Si	SiO_2 (ref. 20); [a]SiO	Si, Si_2, Si_3, SiO, SiO_2 (ref. 20); [b]Si_2O_2
Cr	Cr_2O_3 (ref. 21); [c]CrO_3, CrO_2	Cr, CrO, CrO2 (ref. 22); CrO_3 (ref. 23); [d]Cr_3O_9, Cr_4O_{12}, Cr_5O_{15}; [e]Cr_2
Fe	FeO, Fe_3O_4, Fe_2O_3 (ref. 20)	Fe, FeO (ref. 20); [e]Fe_2
Nb	NbO, NbO_2, Nb_2O_5 (ref. 22)	Nb, NbO, NbO_2 (ref. 22)
Ta	Ta_2O_5 (ref. 22)	Ta, TaO, TaO_2 (ref. 22)
Zr	ZrO_2 (ref. 22)	Zr, ZrO, ZrO_2 (ref. 22)
W	WO_2, WO_3, [f]WO_{3-x} (ref. 20)	W, WO, WO_2, WO_3, W_3O_8, $(WO_3)_2$, $(WO_3)_3$, $(WO_3)_4$ (ref. 20)

[a]No thermodynamic data have been tabulated for the not well characterized metastable SiO(s) phase. Therefore, this phase is not included in the equilibrium calculations.

[b]Although Si_2O_2(g) has been identified in a mass spectrometric study of the vaporization of the Si-SiO_2 system, no thermodynamic data have been tabulated for this species. The results of the mass spectrometric study indicate that this species will be much less abundant ($< 10^{-3}$) than SiO(g) (ref. 24).

[c]The CrO_2 and CrO_3 condensed phases decompose above 800 K (ref. 22).

[d]The gaseous polymers of CrO_3 have been observed mass spectrometrically over CrO_3(s) at low temperatures (< 500 K)(ref. 25). Thermodynamic circumstances indicate that these species are unimportant at the temperatures under consideration in the present study.

[e]The identification of Cr_2(g) and Fe_2(g) have been made by high temperature mass spectrometry (refs. 26 and 27). The results of these investigations show that the concentrations of these molecules are roughly 10^{-6} those of the atomic species at temperatures of 2000 K. Thus, they are not considered in the present study.

[f]Thermodynamic data for the substoichiometric W-O phases $WO_{2.72}$, $WO_{2.90}$, and $WO_{2.96}$ have been tabulated (ref. 20). For purpose of construction of the thermochemical diagrams, however, these are ignored.

TABLE III. - CHEMICAL REACTIONS WHICH PRODUCE THE MAJOR COMPONENTS OF THE VAPOR PHASE

Element	Condensed phase	Major chemical reactions for volatilization
Si	SiO_2	$SiO_2(s) = SiO(g) + 1/2\ O_2(g)$ $SiO_2(s) = SiO_2(g)$
	Si	$Si(s) + 1/2\ O_2(g) = SiO(g)$ $Si(s) = Si(g)$
Cr	Cr_2O_3	$Cr_2O_3(s) + 3/2\ O_2(g) = 2CrO_3(g)$ $Cr_2O_3(s) + 1/2\ O_2(g) = 2CrO_2(g)$ $Cr_2O_3(s) = 2CrO(g) + 1/2\ O_2(g)$ $Cr_2O_3(s) = 2Cr(g) + 3/2\ O_2(g)$
	Cr	$Cr(s) = Cr(g)$
Fe	Fe_2O_3	$Fe_2O_3(s) = 2FeO(g) + 1/2\ O_2(g)$ $Fe_2O_3(s) = 2Fe(g) + 3/2\ O_2(g)$
	Fe_3O_4	$Fe_3O_4(s) = 3FeO(g) + 1/2\ O_2(g)$ $Fe_3O_4(s) = 3Fe(g) + 2\ O_2(g)$
	FeO	$FeO(s) = Fe(g) + 1/2\ O_2(g)$ $FeO(s) = FeO(g)$
	Fe	$Fe(s) = Fe(g)$
Nb	Nb_2O_5	$Nb_2O_5(s) = 2NbO_2(g) + 1/2\ O_2(g)$
	NbO_2	$NbO_2(s) = NbO_2(g)$
	NbO	$NbO(s) + 1/2\ O_2(g) = NbO_2(g)$
	Nb	$Nb(s) + 1/2\ O_2(g) = NbO(g)$ $Nb(s) + O_2(g) = NbO_2(g)$
Ta	Ta_2O_5	$Ta_2O_5(s) = 2TaO_2(g) + 1/2\ O_2(g)$
	Ta	$Ta(s) + 1/2\ O_2(g) = TaO(g)$ $Ta(s) + O_2(g) = TaO_2(g)$
Zr	ZrO_2	$ZrO_2(s) = ZrO_2(g)$ $ZrO_2(s) = ZrO(g) + 1/2\ O_2(g)$
	Zr	$Zr(s) = Zr(g)$ $Zr(s) + 1/2\ O_2(g) = ZrO(g)$
W	WO_3	$3WO_3(s) = (WO_3)_3(g)$ $4WO_3(s) = (WO_3)_4(g)$ $2WO_3(s) = (WO_3)_2(g)$
	WO_2, W	Numerous reactions are important as shown in Fig. 7

TABLE IV. - VALUE OF OXYGEN PRESSURE AT CONDENSED STATE PHASE BOUNDARIES AS A FUNCTION OF TEMPERATURE (1300 TO 1700 K).

Element	Condensed phases	Reaction	Oxygen pressure equation (atm)
Si	$Si-SiO_2$	$Si(s) + O_2(g) = SiO_2(s)$	$\log P_{O_2(g)} = -4.718 \cdot 10^4/T + 9.034$
Cr	$Cr-Cr_2O_3$	$2Cr(s) + 3/2\ O_2(g) = Cr_2O_3(s)$	$\log P_{O_2(g)} = -3.905 \cdot 10^4/T + 8.673$
Fe	$Fe_3O_4-Fe_2O_3$	$2Fe_3O_4(s) + 1/2\ O_2(g) = 3Fe_2O_3(s)$	$\log P_{O_2(g)} = -2.445 \cdot 10^4/T + 14.072$
	$FeO-Fe_3O_4$	$3FeO(s) + 1/2\ O_2(g) = Fe_3O_4(s)$	$\log P_{O_2(g)} = -2.996 \cdot 10^4/T + 11.935$
	Fe-FeO	$Fe(s) + 1/2\ O_2(g) = FeO(s)$	$\log P_{O_2(g)} = -2.795 \cdot 10^4/T + 6.405$
Nb	$NbO_2-Nb_2O_5$	$2NbO_2(s) + 1/2\ O_2(g) = Nb_2O_5(s)$	$\log P_{O_2(g)} = -3.391 \cdot 10^4/T + 9.047$
	$NbO-NbO_2$	$NbO(s) + 1/2\ O_2(g) = NbO_2(s)$	$\log P_{O_2(g)} = -3.856 \cdot 10^4/T + 8.209$
	Nb-NbO	$Nb(s) + 1/2\ O_2(g) = NbO(s)$	$\log P_{O_2(g)} = -4.185 \cdot 10^4/T + 8.453$
Ta	$Ta-Ta_2O_5$	$2Ta(s) + 5/2\ O_2(g) = Ta_2O_5(s)$	$\log P_{O_2(g)} = -4.117 \cdot 10^4/T + 8.361$
Zr	$Zr-ZrO_2$	$Zr(s) + O_2(g) = ZrO_2(s)$	$\log P_{O_2(g)} = -5.651 \cdot 10^4/T + 9.408$
W	WO_2-WO_3	$WO_2(s) + 1/2\ O_2(g) = WO_3(s)$	$\log P_{O_2(g)} = -2.573 \cdot 10^4/T + 7.145$
	$W-WO_2$	$W(s) + O_2(g) = WO_2(s)$	$\log P_{O_2(g)} = -2.982 \cdot 10^4/T + 8.655$

TABLE V. - VAPOR PRESSURES OF MAJOR VAPOR PHASE COMPONENTS AS A FUNCTION OF OXYGEN PRESSURE AND TEMPERATURE (1300 TO 1700 K)

Element	Condensed phase	Vapor pressure equations (atm)
Si	SiO_2	$\log P_{SiO(g)} = -4.124 \cdot 10^4/T + 12.993 - 1/2 \log P_{O_2(g)}$ $\log P_{SiO_2(g)} = -3.083 \cdot 10^4/T + 8.878$
	Si	$\log P_{SiO(g)} = 5.949 \cdot 10^3/T + 3.959 + 1/2 \log P_{O_2(g)}$ $\log P_{Si(g)} = -2.307 \cdot 10^4/T + 7.384$
Cr	Cr_2O_3	$\log P_{CrO_3(g)} = -1.229 \cdot 10^4/T + 3.084 + 3/4 \log P_{O_2(g)}$ $\log P_{CrO_2(g)} = -2.430 \cdot 10^4/T + 7.161 + 1/4 \log P_{O_2(g)}$ $\log P_{CrO(g)} = -3.935 \cdot 10^4/T + 11.408 - 1/4 \log P_{O_2(g)}$ $\log P_{Cr(g)} = -4.924 \cdot 10^4/T + 13.574 - 3/4 \log P_{O_2(g)}$
	Cr	$\log P_{Cr(g)} = -1.996 \cdot 10^4/T + 7.072$
Fe	Fe_2O_3	$\log P_{FeO(g)} = -3.285 \cdot 10^4/T + 10.766 - 1/4 \log P_{O_2(g)}$ $\log P_{Fe(g)} = -4.176 \cdot 10^4/T + 13.352 - 3/4 \log P_{O_2(g)}$
	Fe_3O_4	$\log P_{FeO(g)} = -3.081 \cdot 10^4/T + 9.592 - 1/6 \log P_{O_2(g)}$ $\log P_{Fe(g)} = -3.972 \cdot 10^4/T + 12.178 - 2/3 \log P_{O_2(g)}$
	FeO	$\log P_{Fe(g)} = -3.472 \cdot 10^4/T + 10.186 - 1/2 \log P_{O_2(g)}$ $\log P_{FeO(g)} = -2.581 \cdot 10^4/T + 7.600$
	Fe	$\log P_{Fe(g)} = -2.075 \cdot 10^4/T + 6.984$
Nb	Nb_2O_5	$\log P_{NbO_2(g)} = -3.754 \cdot 10^4/T + 11.196 - 1/4 \log P_{O_2(g)}$
	NbO_2	$\log P_{NbO_2(g)} = -2.906 \cdot 10^4/T + 8.935$
	NbO	$\log P_{NbO_2(g)} = -9.780 \cdot 10^3/T + 4.831 + 1/2 \log P_{O_2(g)}$
	Nb	$\log P_{NbO(g)} = -9.461 \cdot 10^3/T + 4.412 + 1/2 \log P_{O_2(g)}$ $\log P_{NbO_2(g)} = 1.114 \cdot 10^4/T + 0.604 + \log P_{O_2(g)}$
Ta	Ta_2O_5	$\log P_{TaO_2(g)} = -4.174 \cdot 10^4/T + 10.856 - 1/4 \log P_{O_2(g)}$
	Ta	$\log P_{TaO(g)} = -1.077 \cdot 10^4/T + 4.557 + 1/2 \log P_{O_2(g)}$ $\log P_{TaO_2(g)} = 1.047 \cdot 10^4/T + 0.405 + \log P_{O_2(g)}$
Zr	ZrO_2	$\log P_{ZrO_2(g)} = -3.780 \cdot 10^4/T + 8.697$ $\log P_{ZrO(g)} = -6.021 \cdot 10^4/T + 13.516 - 1/2 \log P_{O_2(g)}$
	Zr	$\log P_{Zr(g)} = -3.075 \cdot 10^4/T + 6.949$ $\log P_{ZrO(g)} = -3.698 \cdot 10^3/T + 4.108 + 1/2 \log P_{O_2(g)}$
W	WO_3	$\log P_{(WO_3)_3} = -2.464 \cdot 10^4/T + 12.709$ $\log P_{(WO_3)_4} = -2.777 \cdot 10^4/T + 14.088$ $\log P_{(WO_3)_2} = -2.592 \cdot 10^4/T + 12.507$

E-6704

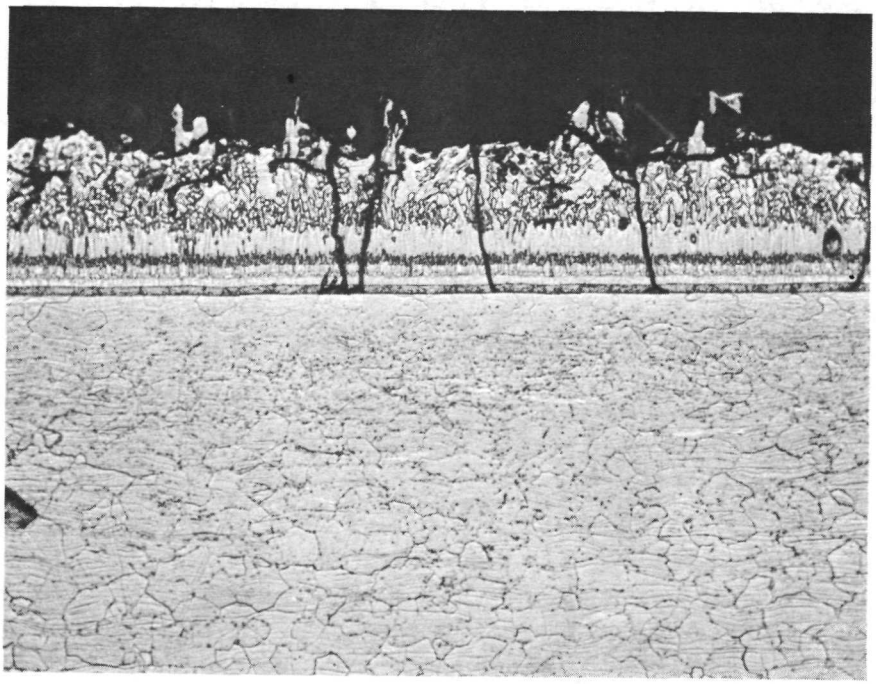

MAGNIFICATION: X250

ETCHANT: HNO_3-HF-Glycerine

Figure 1. Photomicrograph of Si-20Fe-20Cr coated FS-85.

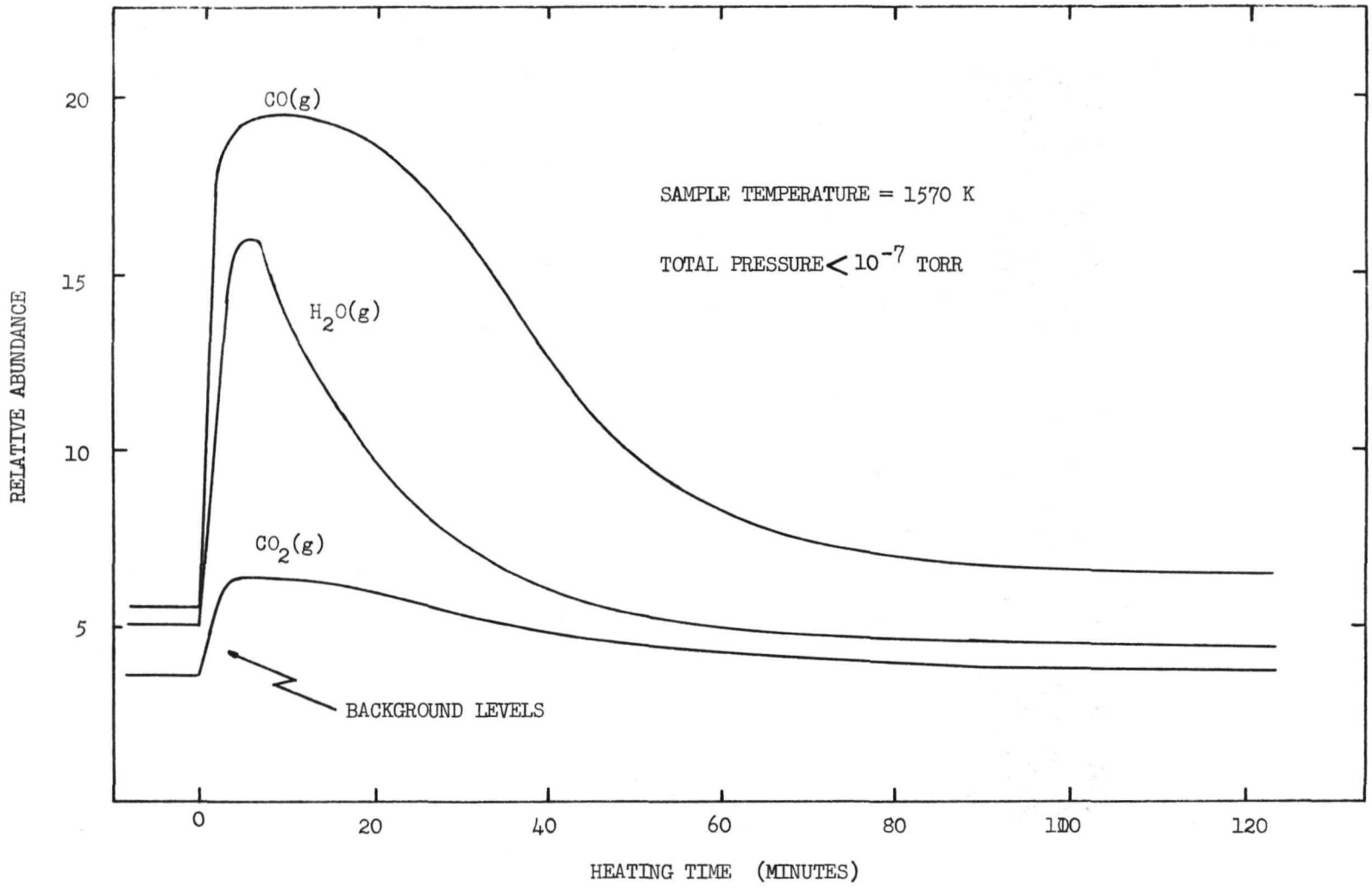

Figure 2. Abundance of mass spectrometrically observed species versus heating time for silicide coated Cb-752 unoxidized.

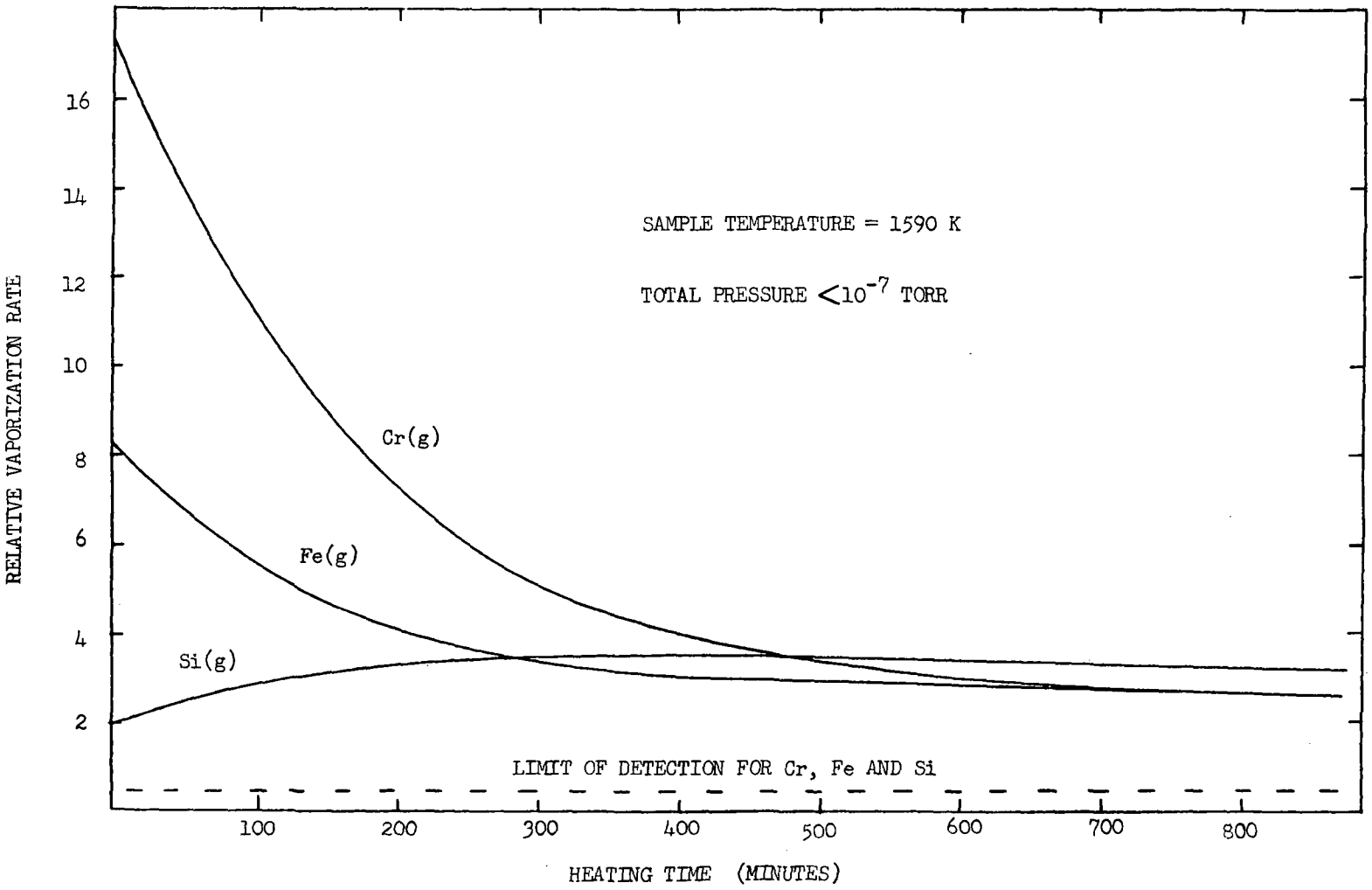

Figure 3. Abundance of mass spectrometrically observed species versus heating time for silicide coated Cb-752 unoxidized.

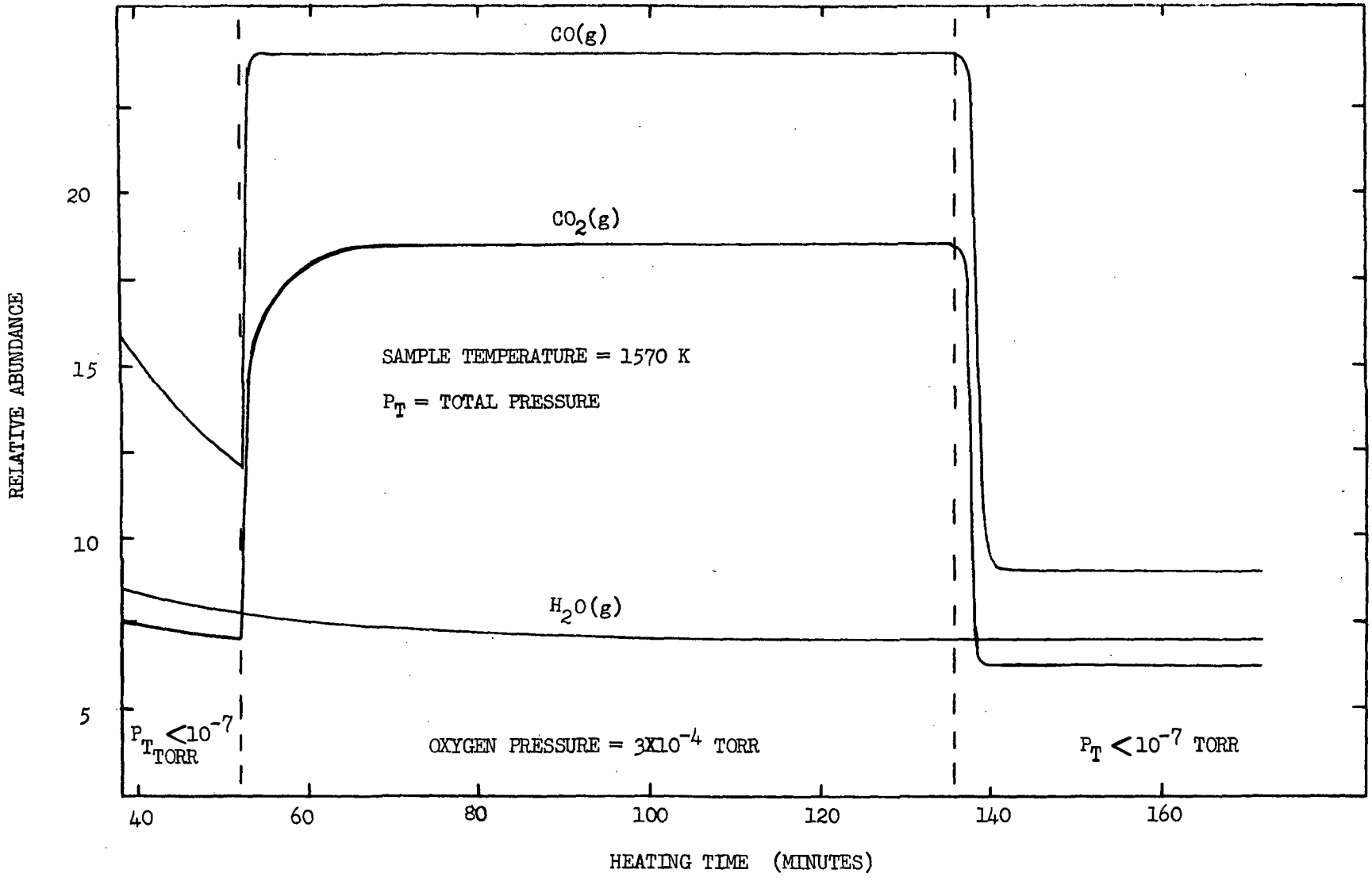

Figure 4. Abundance of mass spectrometrically observed species versus heating time and oxygen exposure for silicide coated Cb-752.

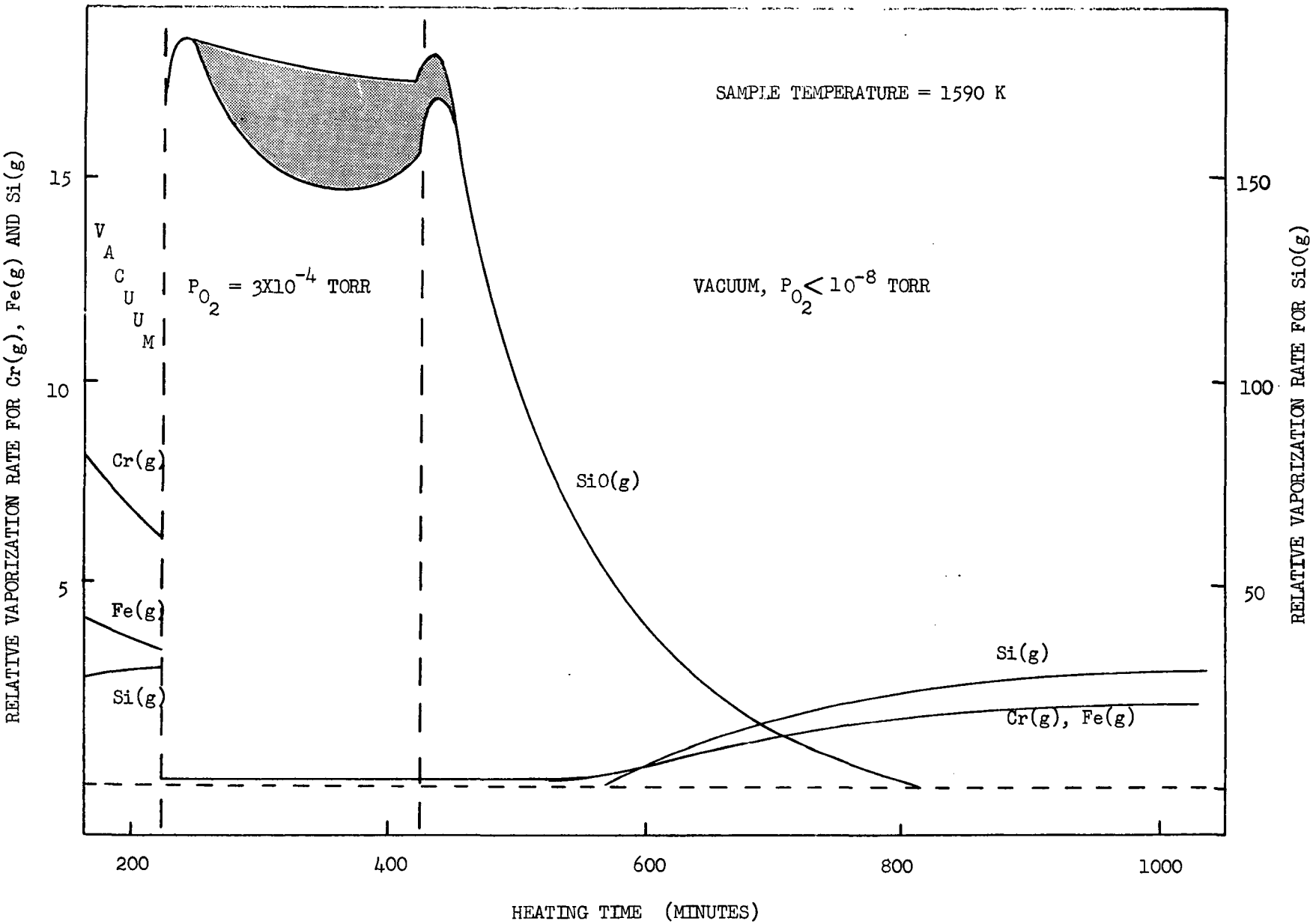

Figure 5. Abundance of mass spectrometrically observed species versus heating time and oxygen exposure for silicide coated Cb-752.

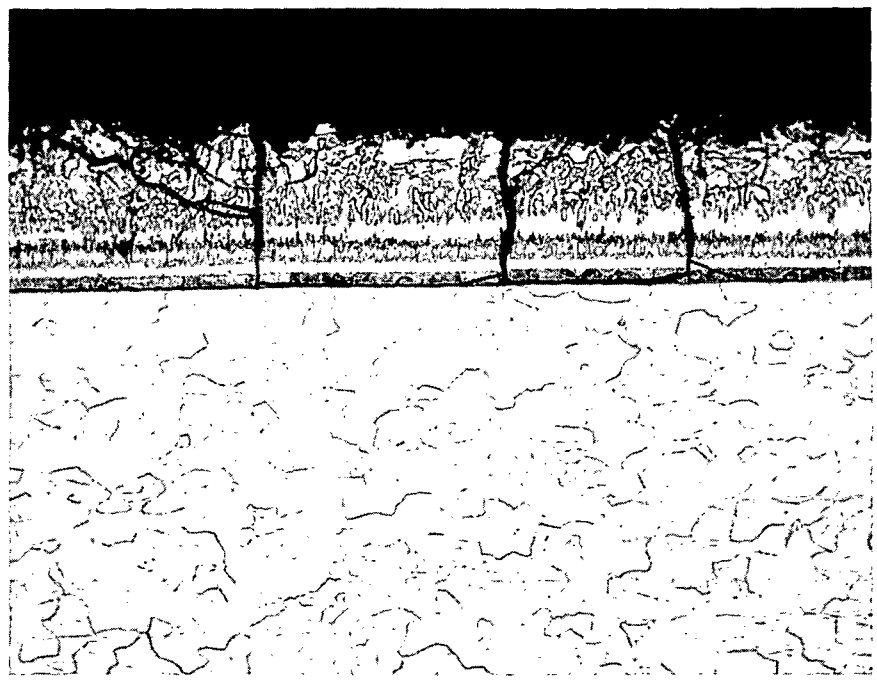

MAGNIFICATION: X250

ETCHANT: HNO_3-HF-Glycerine

Figure 6. Photomicrograph of oxidized Si-20Fe-20Cr coated FS-85 (10 torr oxygen at 1570-1600 K for 6 hours).

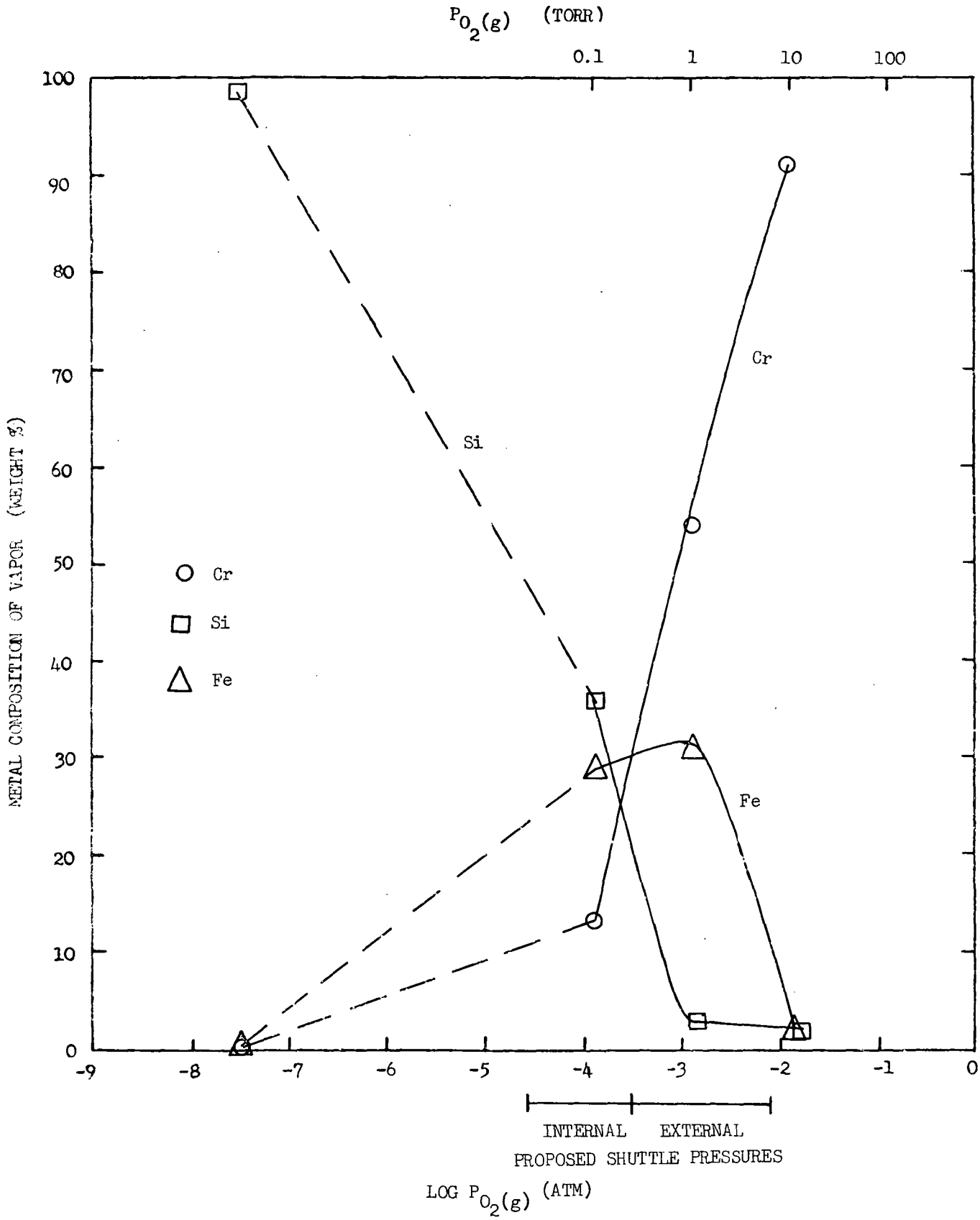

Figure 7. Metal composition of vapor versus oxygen pressure. Points at 10, 1 and 0.1 torr determined by target collection; points at 5×10^{-4} torr determined by mass spectrometry. Si-20Cr-20Fe coated FS-85 at 1570-1600 K.

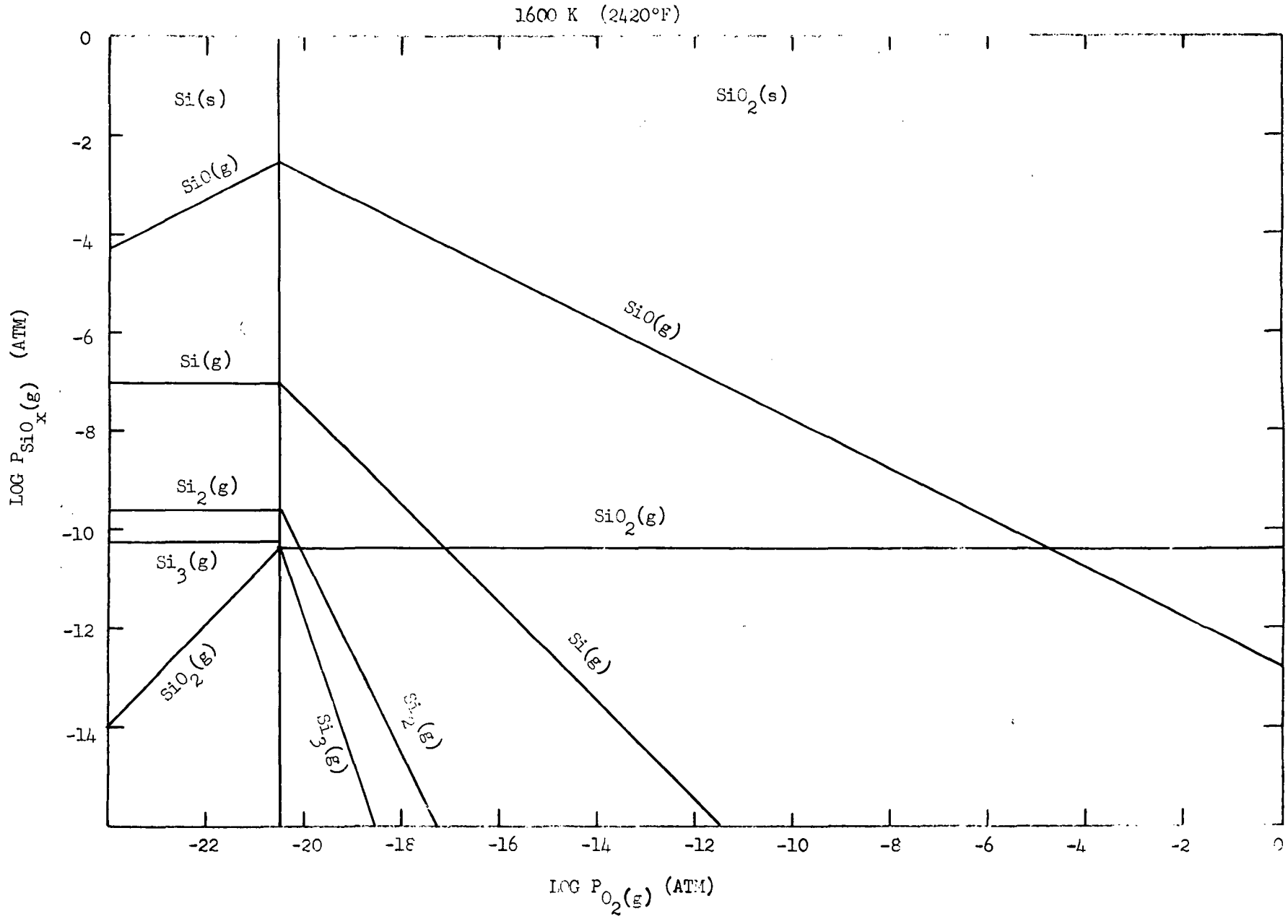

Figure 8. Thermochemical diagram for the silicon-oxygen system at 1600 K.

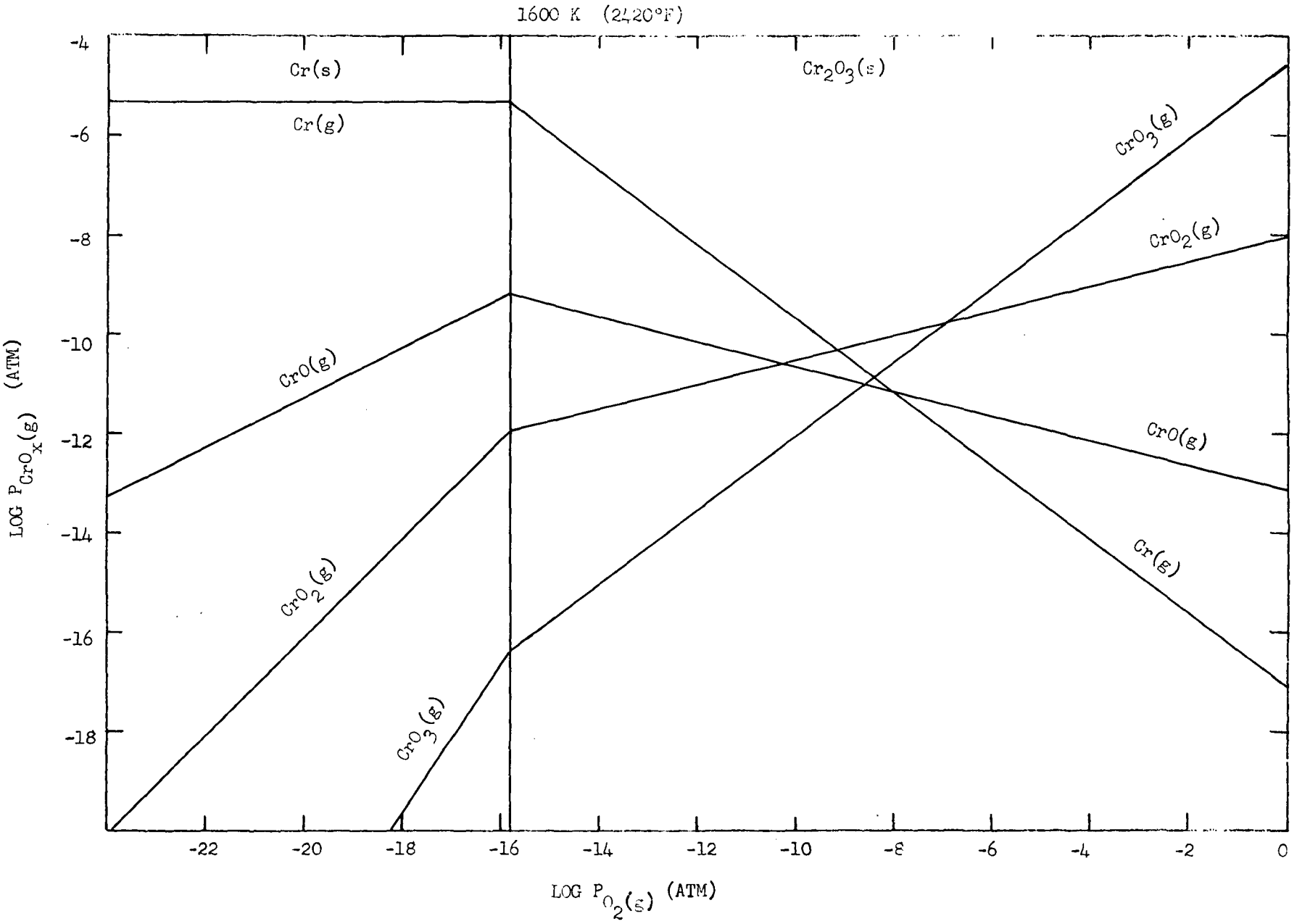

Figure 9. Thermochemical diagram for the chromium-oxygen system at 1600 K.

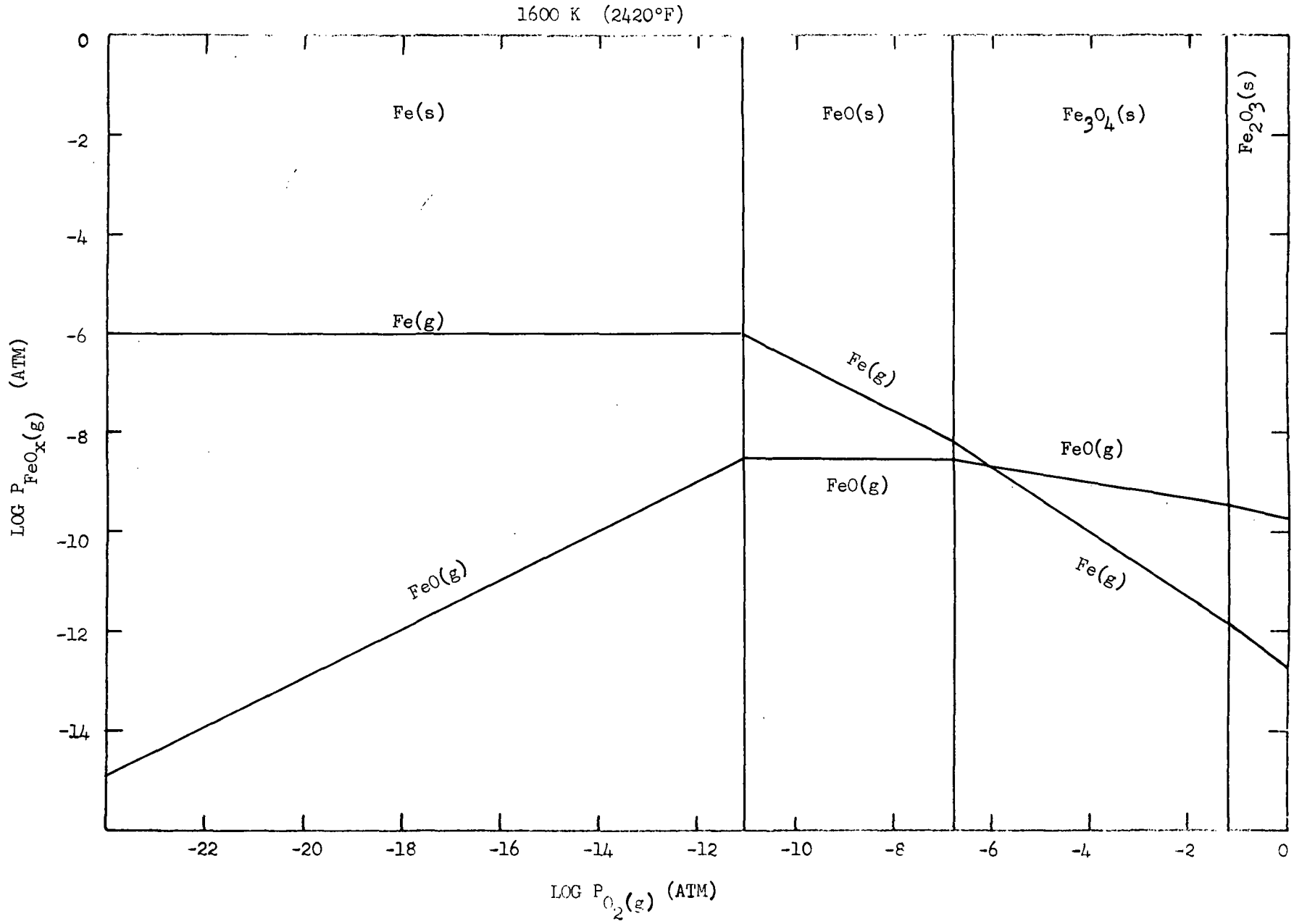

Figure 10. Thermochemical diagram for the iron-oxygen system at 1600 K.

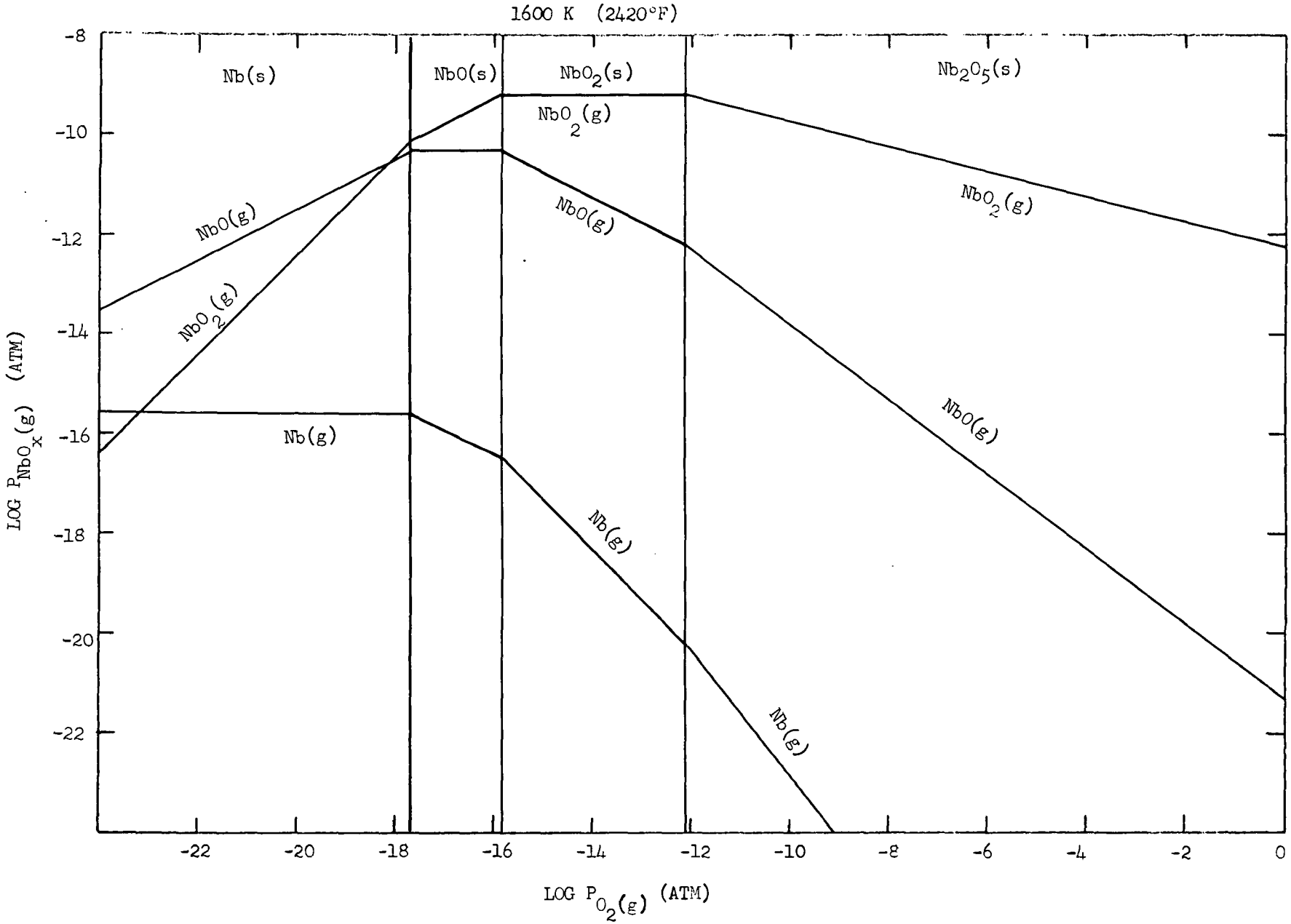

Figure 11. Thermochemical diagram for the columbium-oxygen system at 1600 K.

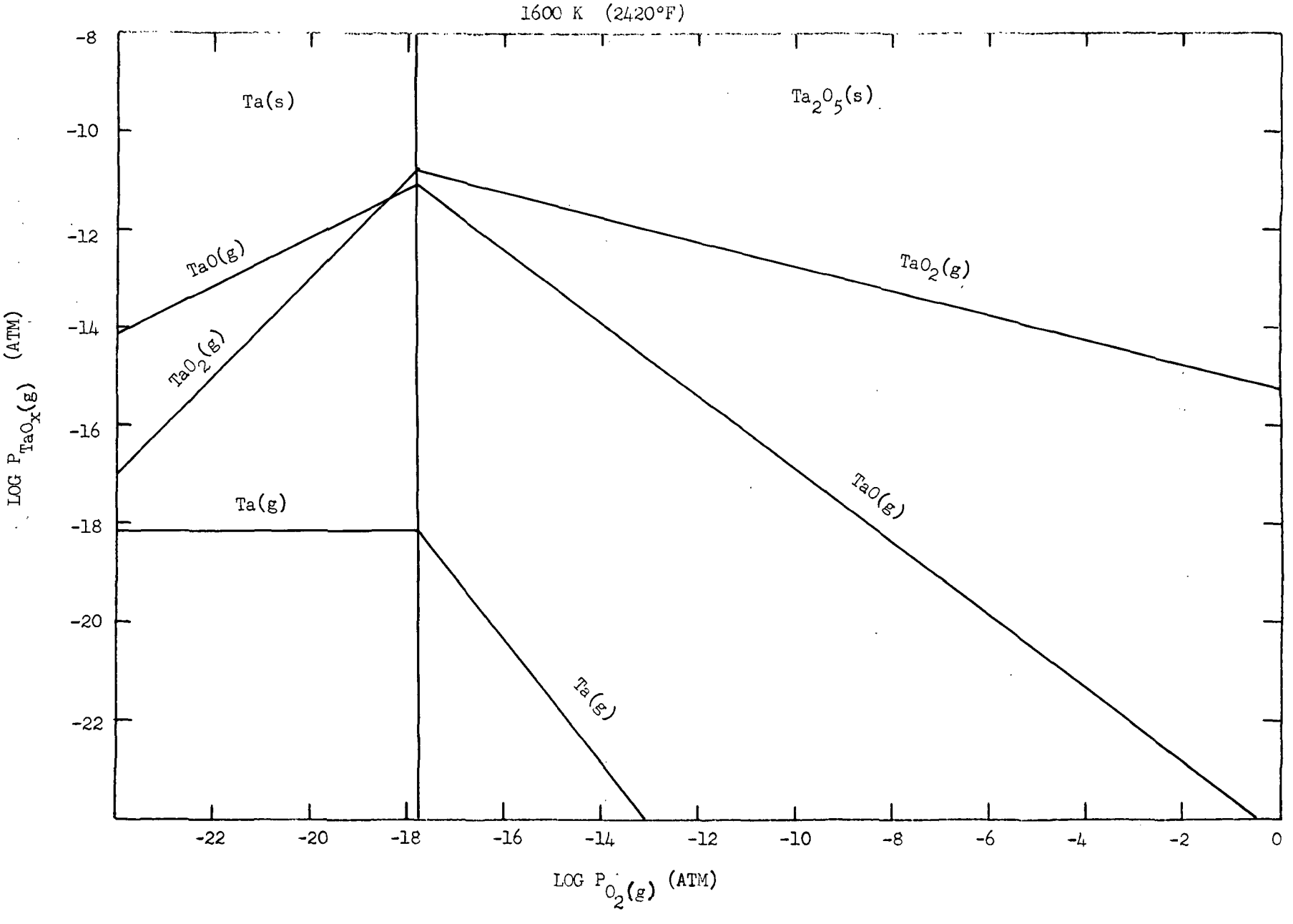

Figure 12. Thermochemical diagram for the tantalum-oxygen system at 1600 K.

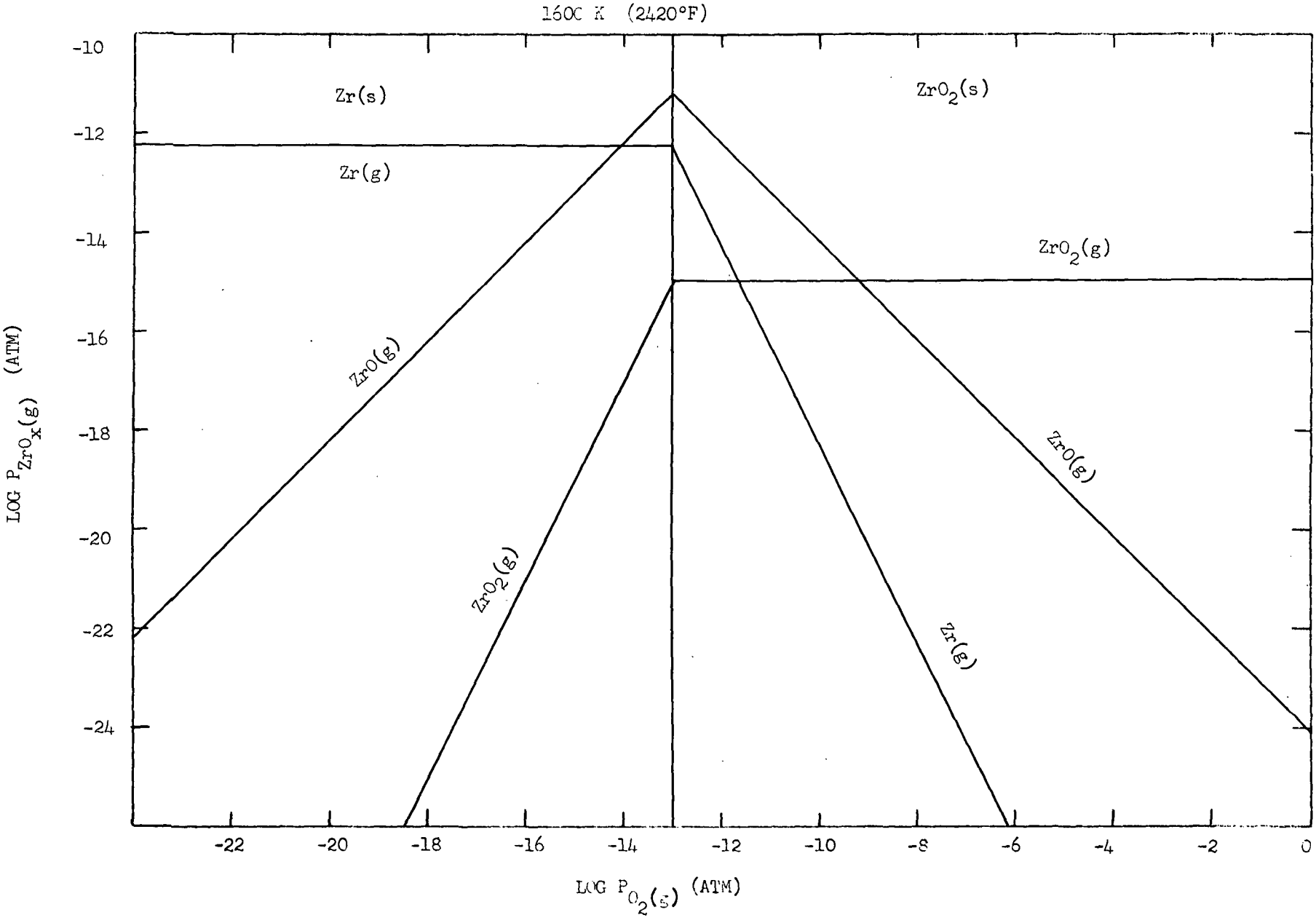

Figure 13. Thermochemical diagram for the zirconium-oxygen system at 1600 K.

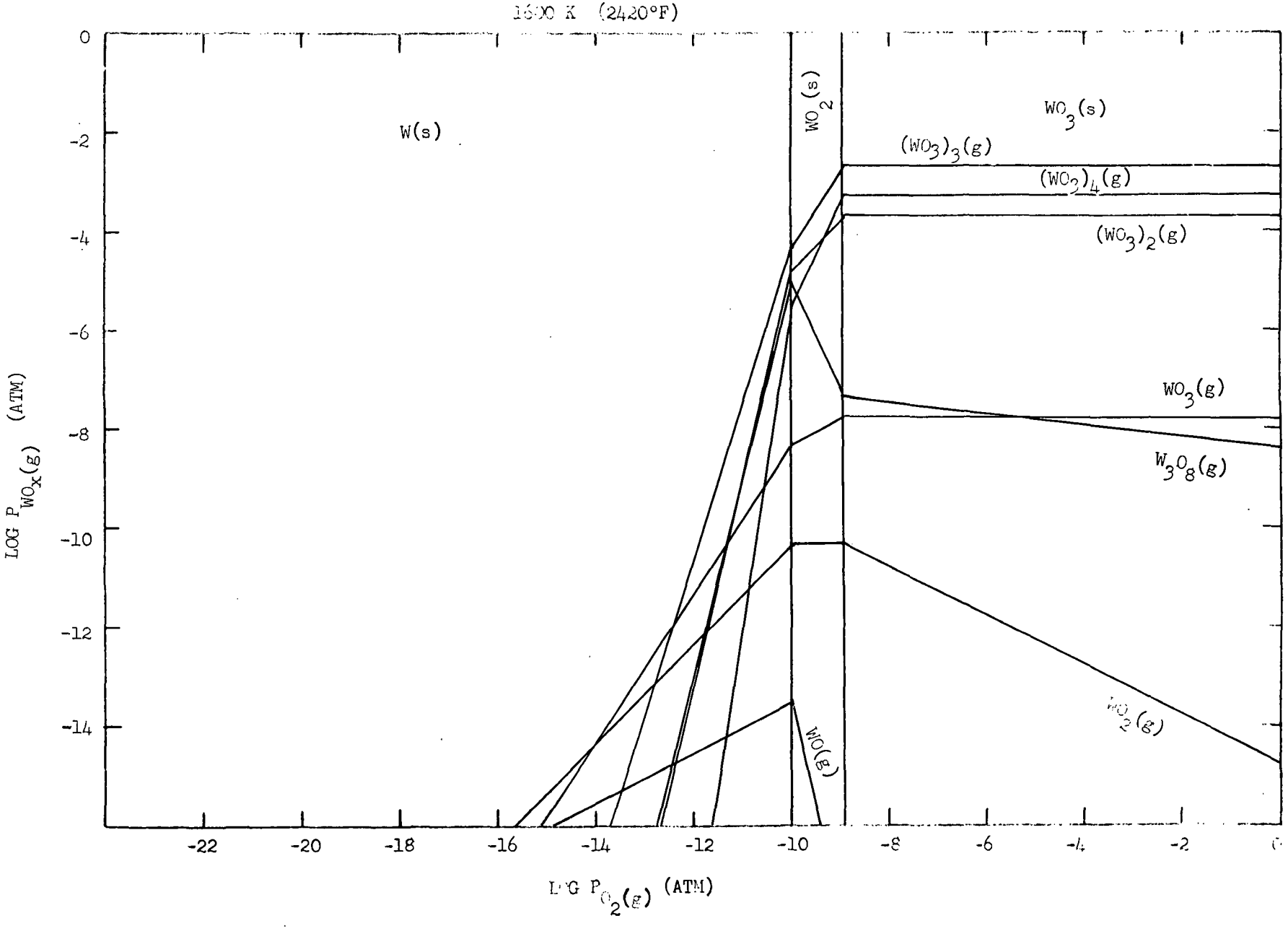

Figure 14. Thermochemical diagram for the tungsten-oxygen system at 1600 K.

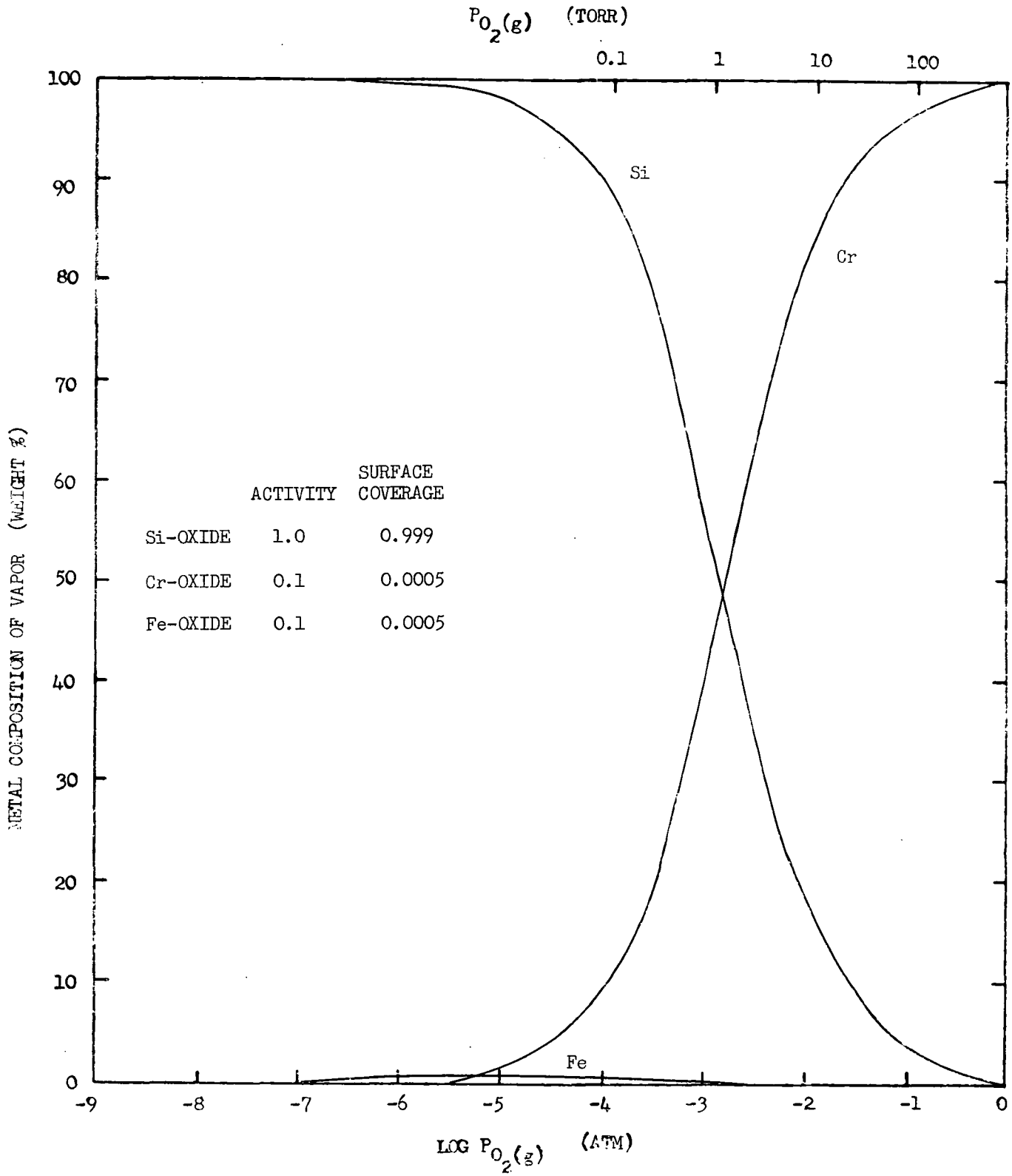

Figure 15. Metal composition of vapor versus oxygen pressure from equilibrium vaporization of oxides of silicon, chromium and iron at 1600 K with activities and surface coverages for oxides as indicated.

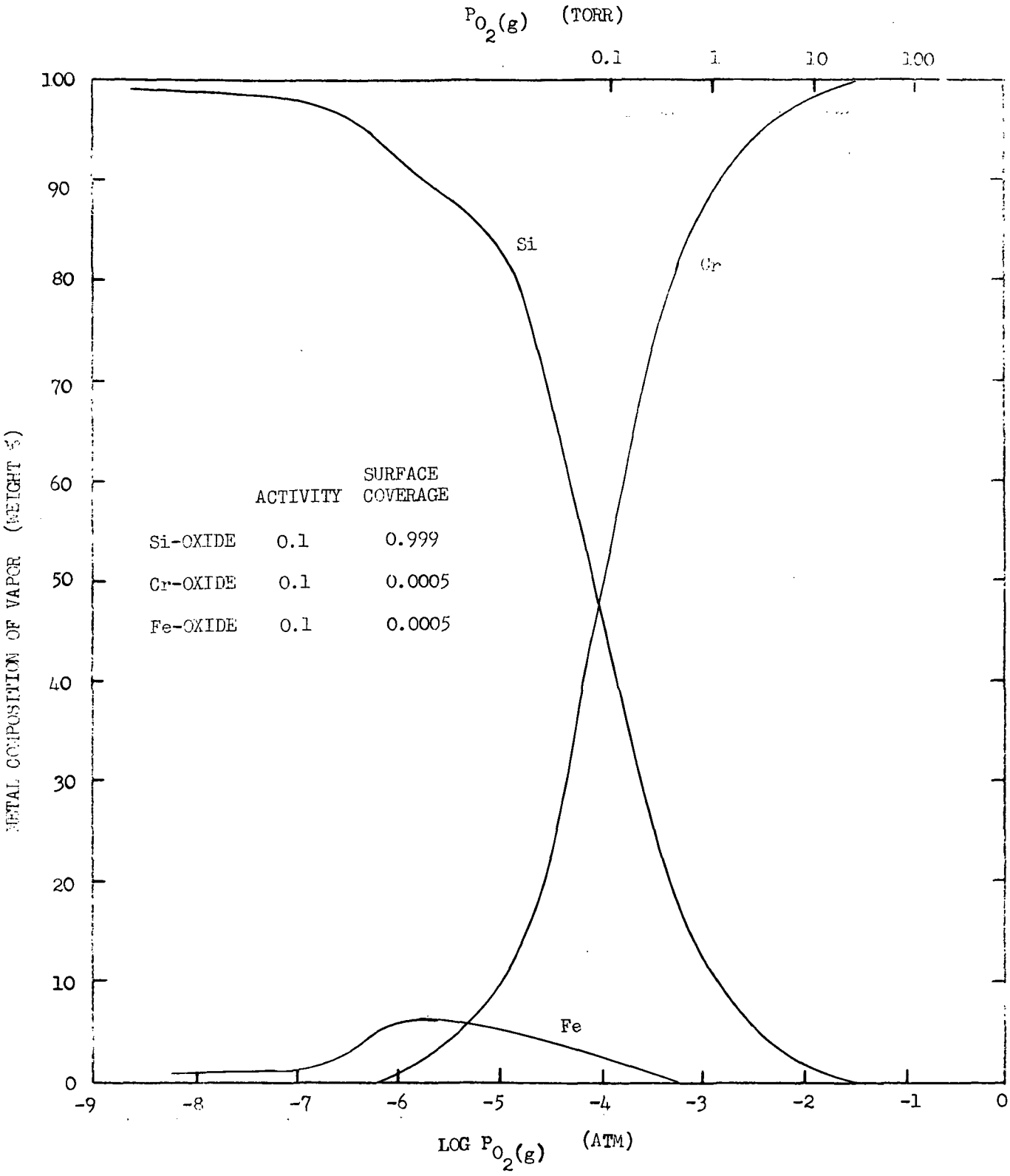

Figure 16. Metal composition of vapor versus oxygen pressure from equilibrium vaporization of oxides of silicon, chromium and iron at 1600 K with activities and surface coverages for oxides as indicated.

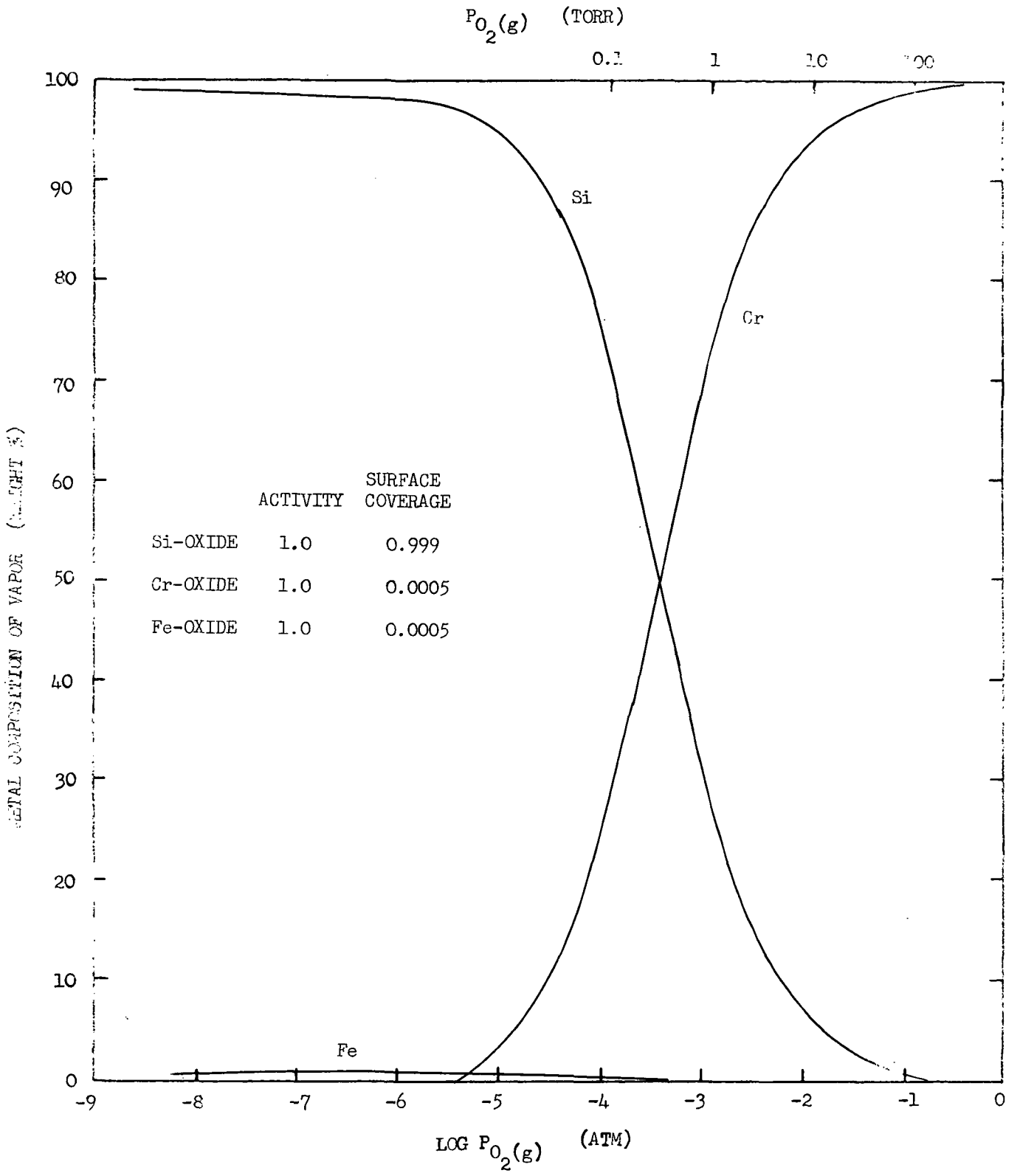

Figure 17. Metal composition of vapor versus oxygen pressure from equilibrium vaporization of oxides of silicon, chromium and iron at 1600 K with activities and surface coverages for oxides as indicated.

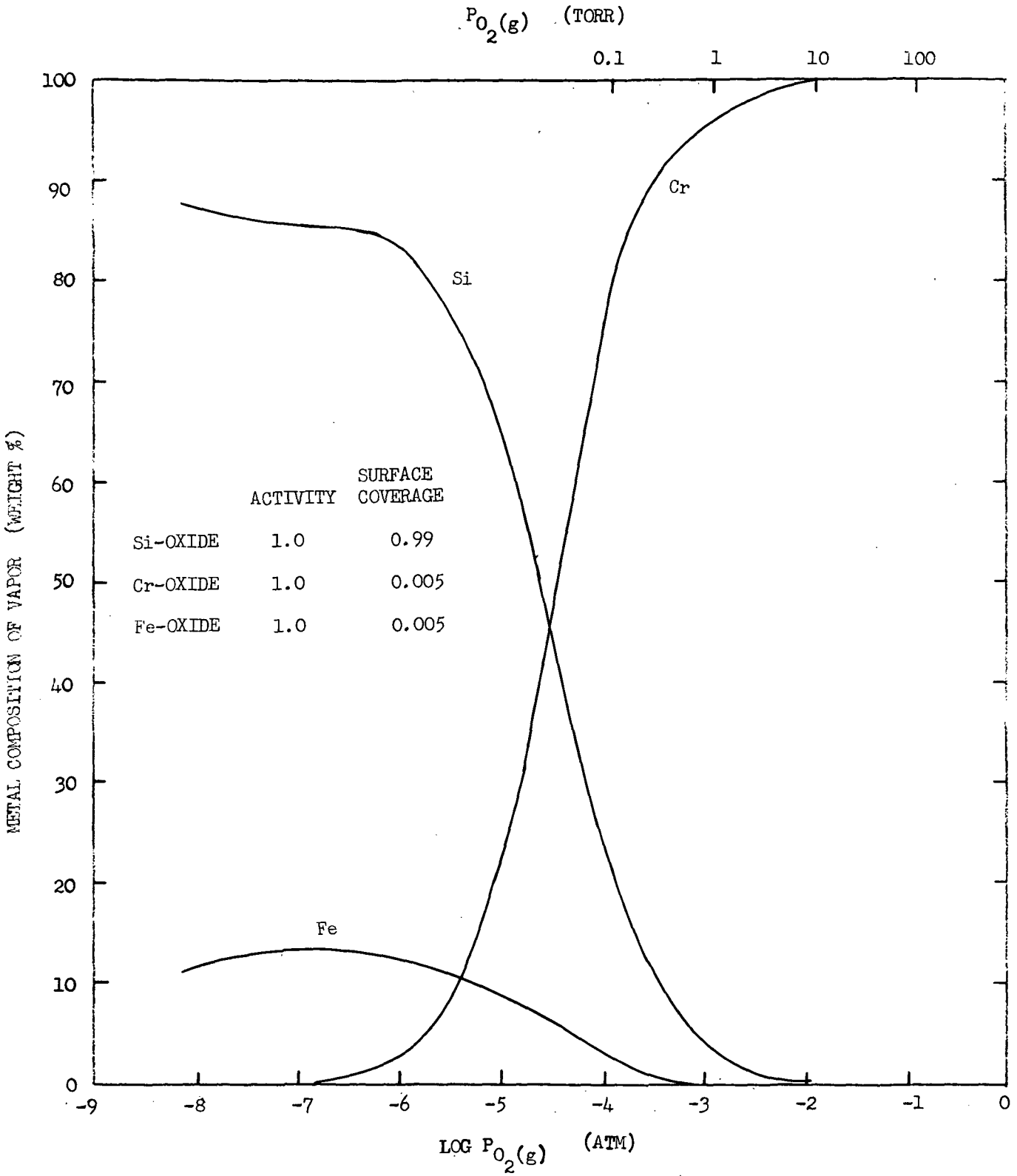

Figure 18. Metal composition of vapor versus oxygen pressure from equilibrium vaporization of oxides of silicon, chromium and iron at 1600 K with activities and surface coverages for oxides as indicated.

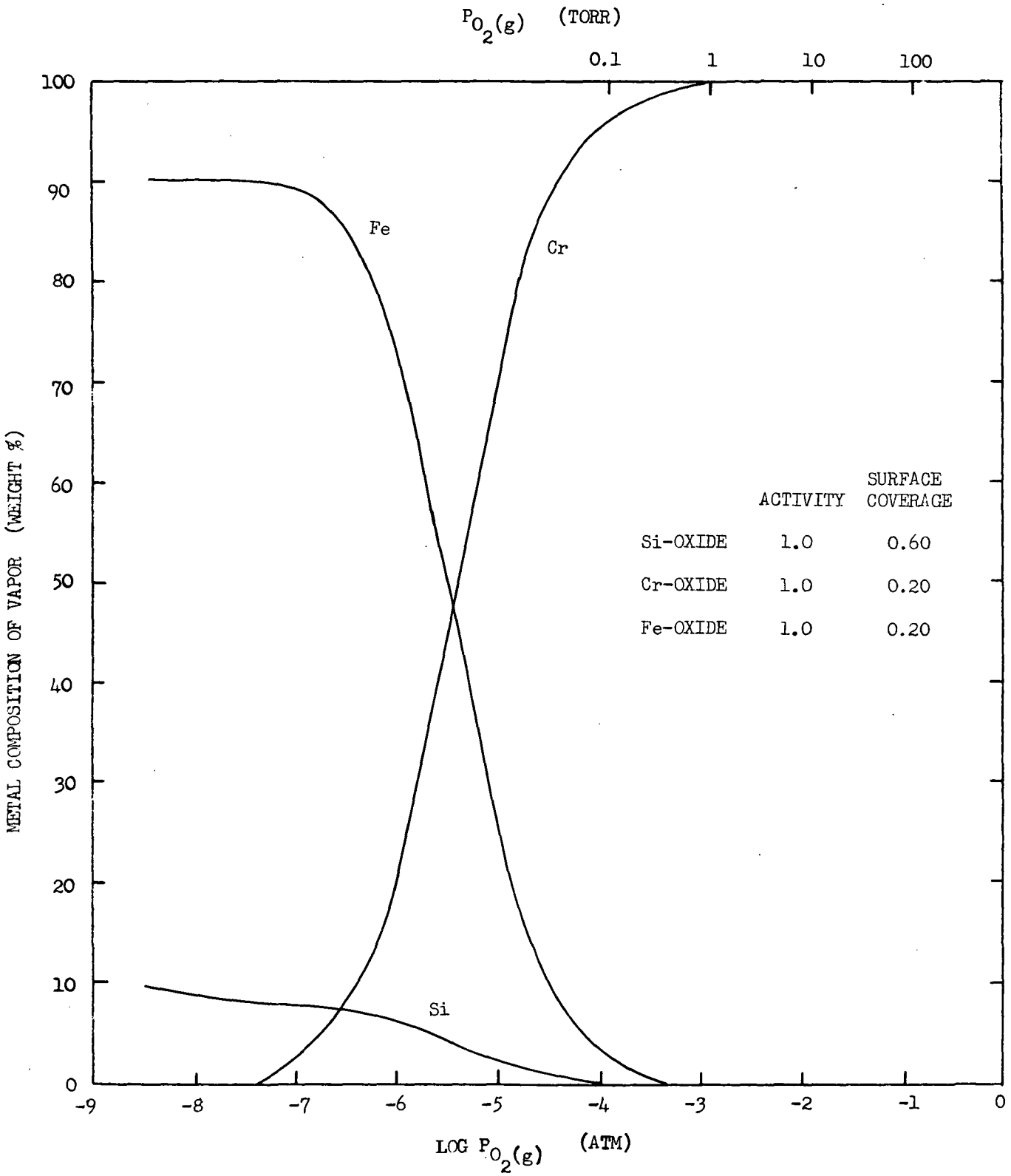

Figure 19. Metal composition of vapor versus oxygen pressure from equilibrium vaporization of oxides of silicon, chromium and iron at 1600 K with activities and surface coverages for oxides as indicated.

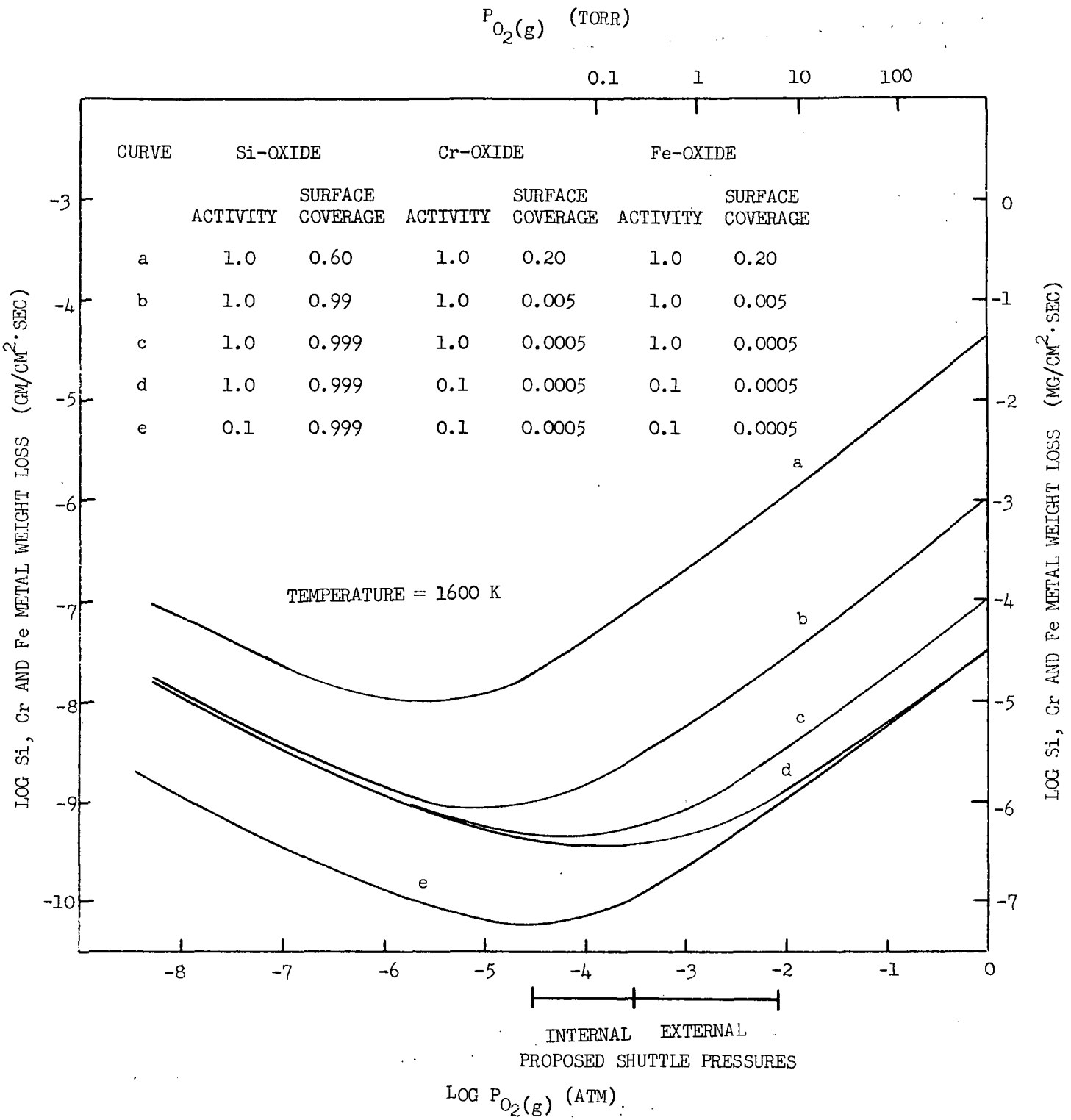

Figure 20. Coating metal weight loss versus oxygen pressure for equilibrium vaporization of oxides of silicon, chromium and iron at 1600 K with activities and surface coverages for oxides as indicated.

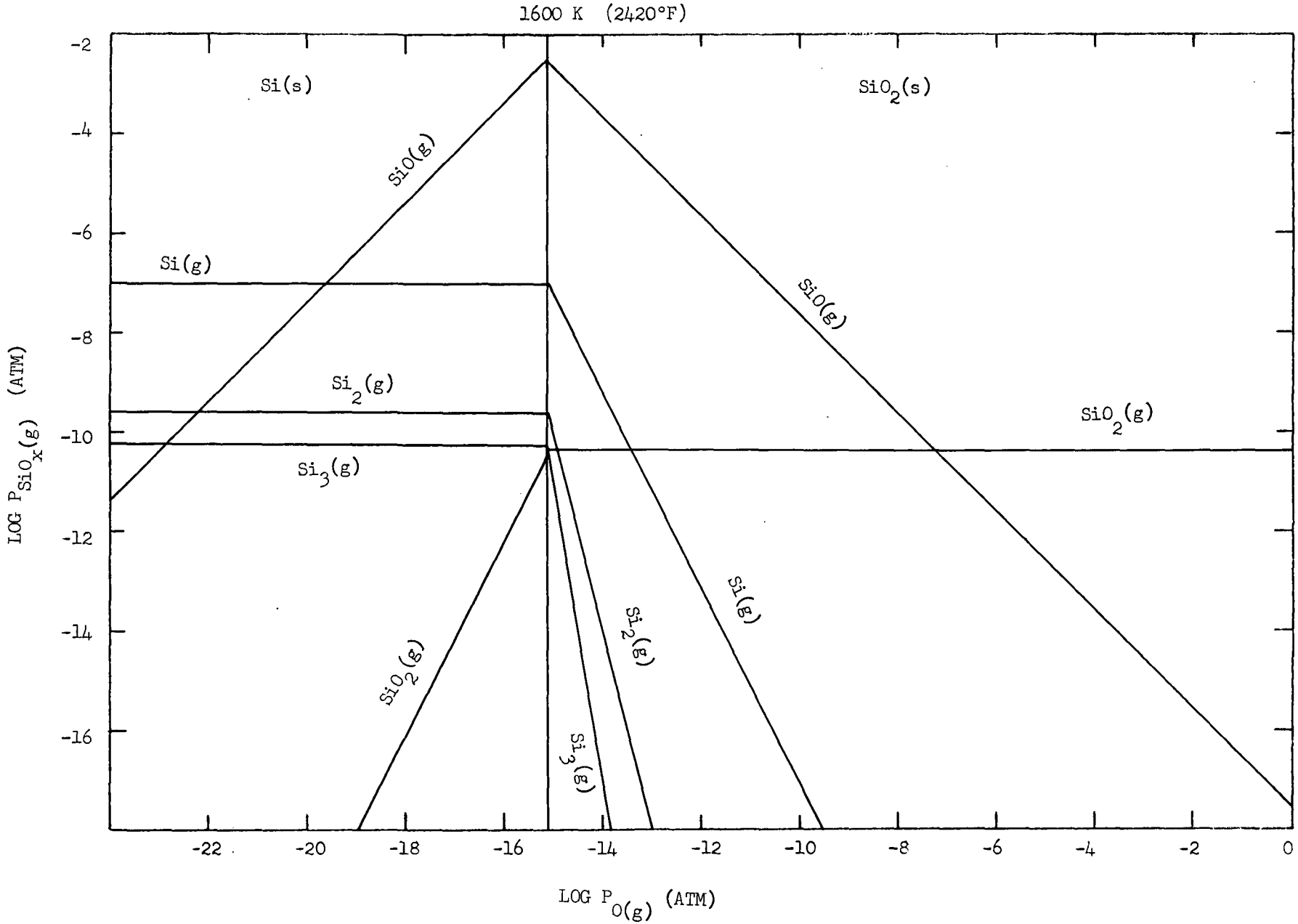

Figure 21. Thermochemical diagram for the silicon-atomic oxygen system at 1600K.

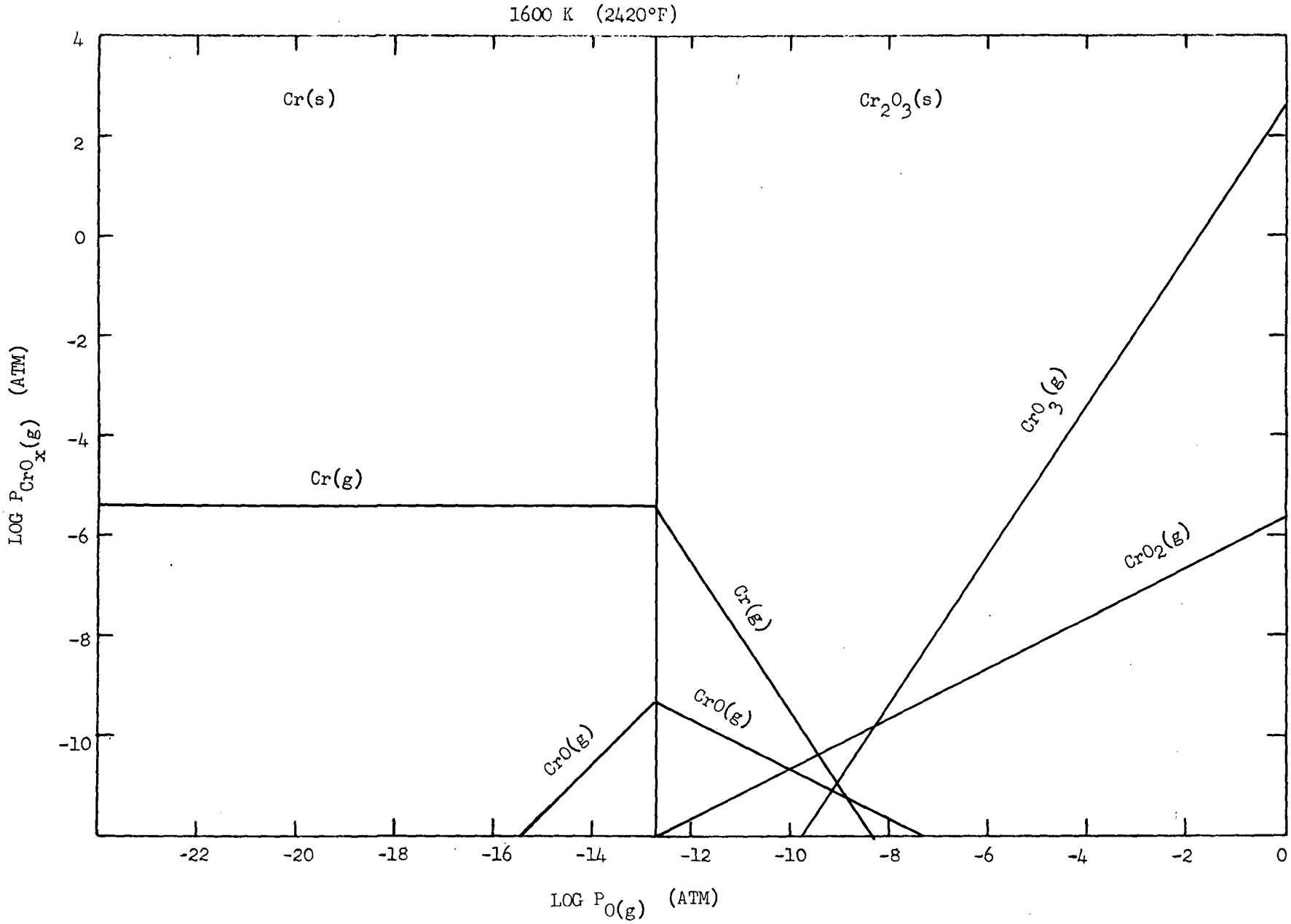

Figure 22. Thermochemical diagram for the chromium-atomic oxygen system at 1600 K.

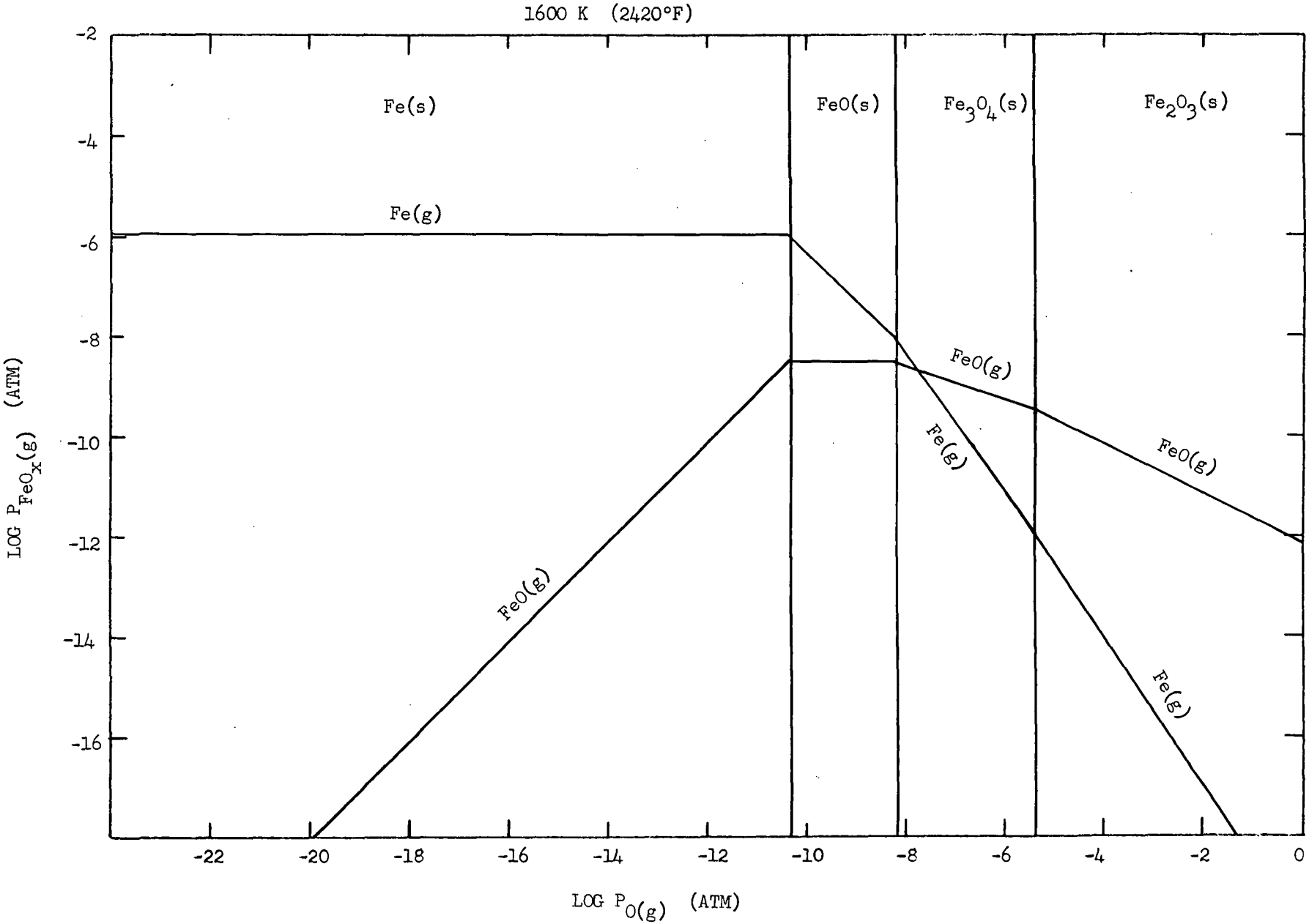

Figure 23. Thermochemical diagram for the iron-atomic oxygen system at 1600 K.